

Piloted Simulation Handling Qualities Assessment of a Business Jet Fly-By-Wire Flight Control System

Tom Berger*

University Affiliated Research Center, Moffett Field, CA

Mark B. Tischler[†]

U.S. Army Aviation Development Directorate–AFDD, Moffett Field, CA

Steven G. Hagerott[‡]

Cessna Aircraft Company, Wichita, KS

A pilot-in-the-loop handling qualities assessment of fly-by-wire control laws for a business jet with a sidestick was conducted in a simulation environment. The control laws were optimized to meet Level 1 requirements for a comprehensive set of stability, handling qualities, and performance specifications. This piloted fixed-based simulation experiment evaluated the control laws using a series of handling qualities demonstration maneuvers, including pitch and roll capture and tracking tasks, as well as an offset landing task. Quantitative performance metrics were collected, in addition to pilot handling qualities ratings and comments. The results show Level 1 handling qualities for the roll tracking and landing tasks, and borderline Level 1 handling qualities for the pitch tracking task. In addition, the fly-by-wire control laws were rated as very predictable and pilots could be more aggressive with a higher level of precision than with the bare-airframe.

Nomenclature

α	Angle-of-attack [deg, rad]
\bar{q}	Dynamic pressure [psf]
β	Angle-of-sideslip [deg, rad]
Δu	Perturbation controls
Δx	Perturbation states
δ_{elev}	Elevator deflection [deg]
δ_{stk}	Stick input
γ	Flightpath angle [deg, rad]
\mathcal{M}	Mass matrix
ω	Frequency [rad/sec]
ω_c	Crossover frequency [rad/sec]
ω_T	Task bandwidth [rad/sec]
ω_{BW}	Aircraft attitude bandwidth [rad/sec]
ω_{co}	Pilot cutoff frequency [rad/sec]
ϕ	Roll attitude [deg, rad]
ψ_β	Dutch roll oscillations phasing angle [deg]
τ	Time delay [sec]

*Research Engineer, University Affiliated Research Center, Senior Member AIAA.

[†]Flight Control Technology Group Leader, Senior Scientist, U.S. Army Aviation Development Directorate–AFDD, Associate Fellow AIAA.

[‡]Senior Engineer Specialist, Aerosciences, Cessna Aircraft Company, Senior Member AIAA.

Approved for public release; distribution is unlimited.

θ	Pitch attitude [deg, rad]
K	Gain
$KCAS_{ref}$	Reference airspeed [kts]
n_z	Normal acceleration [g]
n_{zu}, n_z+u	Normal acceleration plus speed error [g]
p	Roll rate [deg/sec, rad/sec]
q	Pitch rate [deg/sec, rad/sec]
r	Yaw rate [deg/sec, rad/sec]
s	Laplace variable
t	Time [sec]
V_{MCA}	Minimum control speed [kts]
V_{MO}	Maximum operating limit speed [kts]
Y_c	Aircraft response
Y_p	Pilot response
AGL	Above Ground Level
CG	Center of Gravity
DRB	Disturbance Rejection Bandwidth
DRP	Disturbance Rejection Peak
EMF	Explicit Model Following
FBW	Fly-by-Wire
GM	Gain Margin
HQR	Handling Qualities Rating
LOES	Lower Order Equivalent System
LQR	Linear-Quadratic Regulator
MAC	Mean Aerodynamic Chord
PIO	Pilot-Induced Oscillation
PIOR	Pilot-Induced Oscillation Rating
PM	Phase Margin
PVS	Pilot-Vehicle System

I. Introduction

A handling qualities optimization based approach to flight control design was used to develop and evaluate fly-by-wire (FBW) control laws for a small (around 10,000 lb maximum takeoff weight) business jet, similar to a Cessna Citation CJ1. The work was done as part of a joint effort by the U.S. Army Aviation Development Directorate-AFDD, Cessna Aircraft Company, and Aerospace Control Dynamics and presented at the AIAA Atmospheric Flight Mechanics conferences in 2012 for the longitudinal axis¹ and in 2013 for the lateral/directional axes.² The control system optimization, conducted using the Control Designer's Unified Interface (CONDUIT[®]),³ was driven by a comprehensive set of specifications divided into two tiers: Tier 1 specifications were used to drive the optimization, and Tier 2 specifications were used to check many commonly used alternative requirements for the completed design. This two-tiered specification approach was motivated by several comprehensive compendiums of flight control design experience and lessons learned, which emphasize the importance of meeting multi-tier handling qualities and flight control criteria in the design phase for improved safety (e.g. RTO,⁴ Pratt⁵), and in order to avoid pilot-induced oscillations (PIO).

As with the development of any new control system, the aircraft needs to be evaluated using high-gain, pilot-in-the-loop tasks to ensure that the predicted handling qualities Level has been achieved,⁶ and that no handling qualities "cliffs" are present. Therefore, a piloted simulation was conducted at Cessna's fixed-based business jet simulator with the following objectives. First, to evaluate and quantify the handling qualities of the FBW control laws, in order to validate the optimization approach used for flight control design. Second, to ensure that the closed-loop handling characteristics exhibit classical airplane response types that do not require pilot re-training or adaptation, and to verify that the control laws do not exhibit any unusual responses or PIO tendencies while performing operationally relevant as well as high gain tasks. And finally, to quantify the benefits of the FBW control system over the bare-airframe. The tasks used to demonstrate these objectives were selected from MIL-STD-1797B⁶ and an Air Force technical report cataloging handling qualities maneuvers for fixed-wing aircraft,⁷ and include such tasks as offset landing and

pitch and roll tracking.

In support of this experiment, a simulation model of a light business jet similar to a CJ1 was developed, which includes a continuous full-flight envelope (“stitched”) model⁸ of the bare-airframe, built up from discrete linear models and trim values extracted from DARcorporation’s Advanced Aircraft Analysis (AAA)⁹ at 66 flight conditions. Along with the stitched model, the FBW control laws were integrated into the simulation model using gain schedule and trim lookup tables.

The remainder of the paper will cover a description of the aircraft model and the FBW control system that were used, including implementation of the gain schedule. Next, details of the test including a description of the simulator and handling qualities test maneuvers, will be provided. Then, the results of the experiment will be presented, followed by a discussion and conclusions.

II. Simulation Model

A. Aircraft Model

1. Bare-Airframe

The bare-airframe model used in this study is of a light business jet similar to the Cessna Citation CJ1, or Model 525, shown in Figure 1. The model is a twin turboprop-powered business jet which can carry three to nine passengers. It has a maximum takeoff weight (MTOW) of 10,700 lbs, a cruise speed of 389 KTAS, a maximum range of about 1,300 nm, and a service ceiling of 41,000 ft. For this study, the control inceptors used were a sidestick and conventional pedals and throttles. Also, it was assumed that the control surfaces are driven by hydraulic actuators (with representative position and rate limits), and a full authority FBW control system.

For the development of the control laws, linear, point models of the aircraft at different combinations of Mach, flight altitude, weight, and center of gravity (CG) were estimated using AAA software.⁹ The control laws were optimized at 66 different Mach and altitude combinations. At each of these 66 design points, 13 different weight and CG combinations were considered to check robustness, for a total of over 850 models. All models used for control law development are for flaps-up, gear-up cruise configurations. Figure 2(a) shows the different Mach and altitude combinations, as well as the aircraft flight envelope.¹⁰ Figure 2(b) shows the different weight and CG combinations, as well as the aircraft weight-CG envelope.¹⁰

For the piloted simulation evaluation, a continuous, full-envelope model is needed, in lieu of the individual point models. This was accomplished using the model stitching technique,^{8,11} which refers to the process of combining a collection of linear state-space models at various flight conditions with trim data into a full-envelope simulation model. As shown in Figure 3, model stitching is accomplished by implementing lookup tables of the aircraft state trim values, control input trim values, and stability and control derivatives with respect to total instantaneous x-body axis relative velocity, U , based on the point models and trim data extracted from the AAA nonlinear simulation model. Trim states and controls are used to determine perturbation states (Δx) and controls (Δu), which in turn are multiplied by the mass matrix and stability and control derivatives ($\mathcal{M}\Delta u$ and $\mathcal{M}B\Delta x$) to determine perturbation aerodynamic and control forces and moments. The aerodynamic trim forces and moments are then summed to the perturbation values to yield the total aerodynamic forces and moments acting on the aircraft in body axes. In addition, the linearized Coriolis terms (e.g. W_0q , etc., due to formulating equations of motion in body axes) and linearized gravity terms normally included in the A and B state-space matrices are removed and added downstream in their nonlinear form. In essence, model stitching produces a nonlinear simulation model with continuous linear aerodynamics.

The implementation of the CJ1 stitched model includes the accurate characterization of aircraft trim states and dynamics responses as a function of airspeed, altitude, and flap deflection. Additional features in the simulation model include the ability to simulate changes in mass, CG, and inertia, as well as landing gear, takeoff and landing, spoilers, an engine out condition, and different levels of turbulence. The resulting model is accurate for typical aircraft flight dynamics over the entire maneuvering flight regime, except for extreme conditions (e.g. stall or spin).

A more complete description of the bare-airframe stitched model used in this study is provided by Tobias et al.¹¹ Tobias also presents the results of a simulation fidelity test using back-to-back flight and simulator testing, which show excellent agreement in pilot control strategy and workload between the stitched model and actual aircraft.



Figure 1. Typical light business jet—Cessna Citation CJ1.

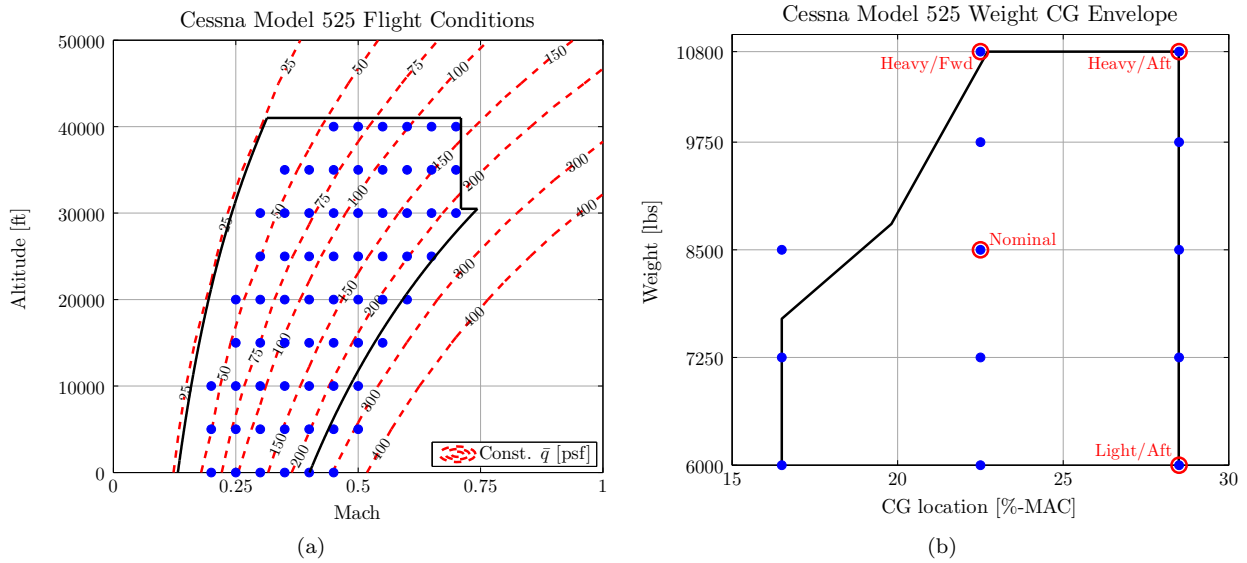


Figure 2. Aircraft (a) flight and (b) loading conditions and envelopes.

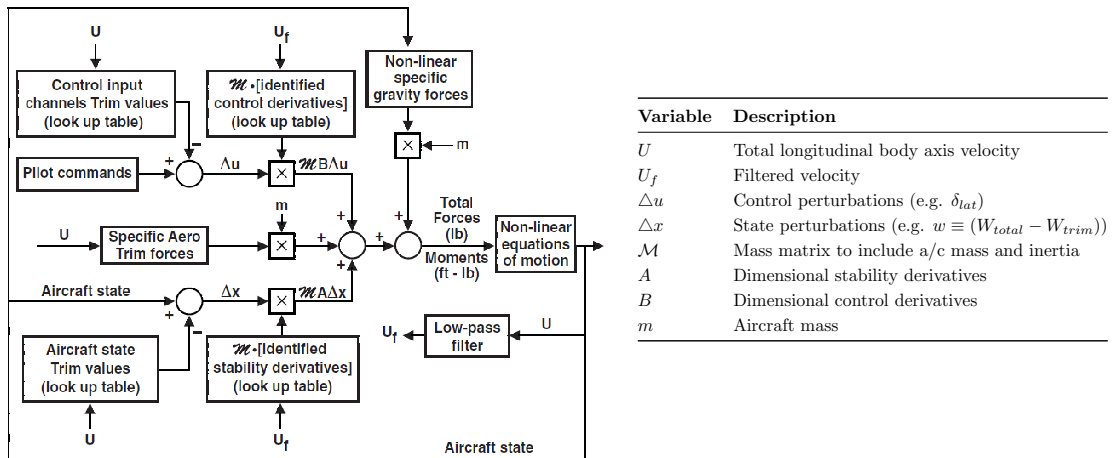


Figure 3. Model stitching block diagram.

2. Actuator and Engine Models

The simulation model includes models of the hydraulic actuators driving the bare-airframe control surfaces. The actuators are represented as second-order systems with position and rate limits. The engine models used were also second-order systems with thrust and thrust rate limits scheduled with Mach and altitude.

B. Control Laws

In both the longitudinal and lateral/directional axes, feed-forward control law gains were explicitly determined to achieve good handling qualities by exploiting parallels between the fixed-wing control laws used and an explicit model following architecture. Feedback gains in the control laws were optimized in CONDUIT[®] using a multi-objective optimization method. The optimization proved capable of determining designs which concurrently met a large number of frequency- and time-domain specifications for both nominal and off-nominal models, while minimizing over-design (i.e. most economical use of actuators and minimizing sensitivity to noise). Furthermore, at each design point, the performance robustness of the control laws was ensured by using a multi-model optimization approach requiring key specifications to be met for the full range of weight/CG configurations, and by enforcing a minimum broken-loop crossover frequency in each control law axis. This allowed the scheduling of the optimized control laws solely with Mach and dynamic pressure resulting in a smooth gain schedule, while still meeting the requirements for the range of weight/CG configurations.^{1,2}

The following sections will give a brief overview of the control laws, as well as updates that were made to the control laws for use with the continuous, full-envelope simulation model.

1. Longitudinal Control Laws

The longitudinal axis control law architecture is shown in simple form in Figure 4. The control laws are referred to as “ $n_z u$ ”-command,¹² i.e. in addition to the stability axes normal acceleration (n_z) command from the pre-filter, a speed error is passed through the feedback integrator. This additional speed error feedback loop provides positive speed stability to the aircraft response, where a pure n_z -command system would otherwise exhibit neutral speed stability. Furthermore, it provides the control laws with two frequency-split command types. At low frequency ($\omega < 0.1$ rad/sec), the pilot stick commands airspeed, while at the mid-frequency range ($0.1 < \omega < 10$ rad/sec), the pilot stick commands normal acceleration, thus preserving

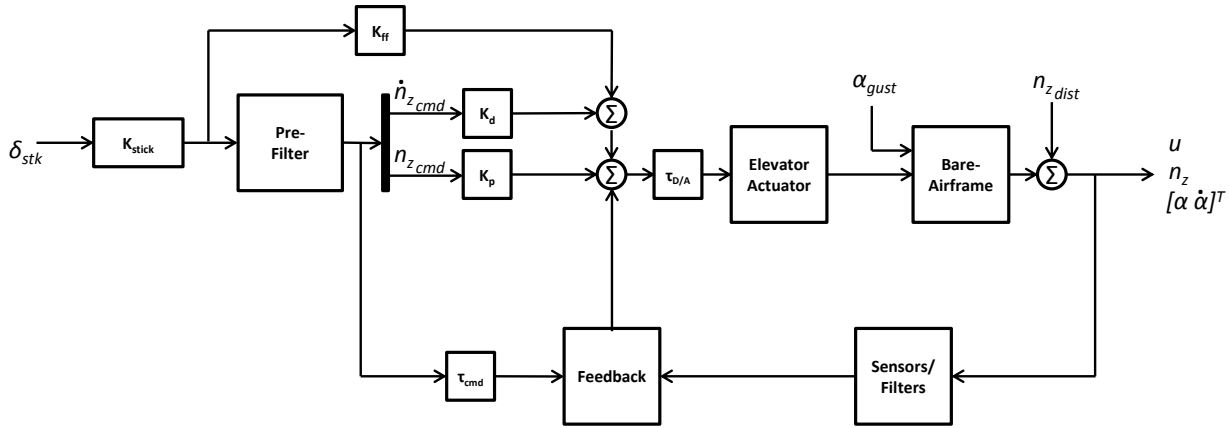


Figure 4. Schematic of longitudinal control law block diagram.

The feed-forward path in Figure 4, comprised of the direct column to elevator path, as well as the second-order pre-filter, was optimized to meet the handling qualities requirements, while the feedback path,

comprised of normal acceleration, angle-of-attack, and angle-of-attack rate, was optimized to meet the stability, short-period frequency and damping, gust rejection, and performance robustness requirements. A total of 21 Level 1 specifications were enforced for each of the 66 design points.

Figure 5 shows the short-term response of the aircraft to a five-second pilot pulse input. The responses are shown for one flight condition (Mach 0.3/5000 ft) and 13 different weight/CG configurations. The aircraft dropback response shown meets the Level 1 requirement.

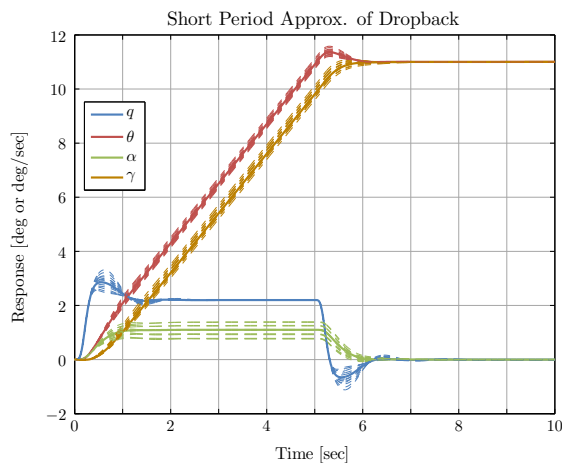


Figure 5. Time history response to a 5-second pulse stick input using short-period bare-airframe dynamics (Mach 0.3/5000 ft flight condition; All weight/CG configurations).

2. Lateral/Directional Control Laws

The lateral/directional axis control law architecture is referred to as “ p - β ”-command, i.e. stability axes roll rate command in the lateral axis and sideslip command in the directional axis.^{14,15} The architecture is shown in simple form in Figure 6. The feed-forward paths in Figure 6, are comprised of the direct stick to aileron path and a first-order pre-filter in the lateral axis, and a direct pedal to rudder path and a second-order pre-filter in the directional axis. As in the longitudinal axis, the feed-forward paths were optimized to meet the handling qualities requirements, while the feedback paths, comprised of stability axes roll rate, sideslip, and sideslip rate, were optimized to meet the stability, damping, gust rejection, and performance robustness requirements. Cross-feed gains, from the directional axis feedback and feed-forward paths to the aileron actuator and from the lateral axis feedback and feed-forward paths to the rudder actuator, were used to tune the off-axis responses to meet handling qualities and gust rejection requirements. A total of 30 Level 1 specifications were enforced for each of the 66 design points.

Figure 7 shows a lateral stick 1-second pulse response of all weight/CG configurations at the Mach 0.3/5000 ft flight condition. The aircraft exhibits a first-order roll rate response, which is expected for a first-order command model. The sideslip response is small, and meets the sideslip excursion specification from MIL-STD-1797B. Figure 8 shows the pedal step response of all weight/CG configurations at the Mach 0.3/5000 ft flight condition. The sideslip response is second-order. The off-axis bank angle response can be tailored using the feed-forward cross-feed gains. In this case, the gains were tuned to give about 1 deg of bank angle for 15 deg of sideslip. The gains were also tuned to remove the non-minimum phase characteristic of roll rate response to rudder deflection, as exhibited by the bare-airframe.

3. Gain Schedule Implementation

A smooth gain schedule was provided by CONDUIT[®] optimization^{1,2} (without requiring further smoothing), and was implemented in a 2D lookup table for each gain as a function of Mach and dynamic pressure. As the short-period dynamics of the bare-airframe do not vary significantly with flap deflection, the control system gains are not scheduled as a function of flap deflection. Figures 9 and 10 show the gain schedules for one of the longitudinal axis feedback gains and one of the lateral axis feedback gains, respectively. The points are connected to show the linear interpolation scheme used by the lookup table.

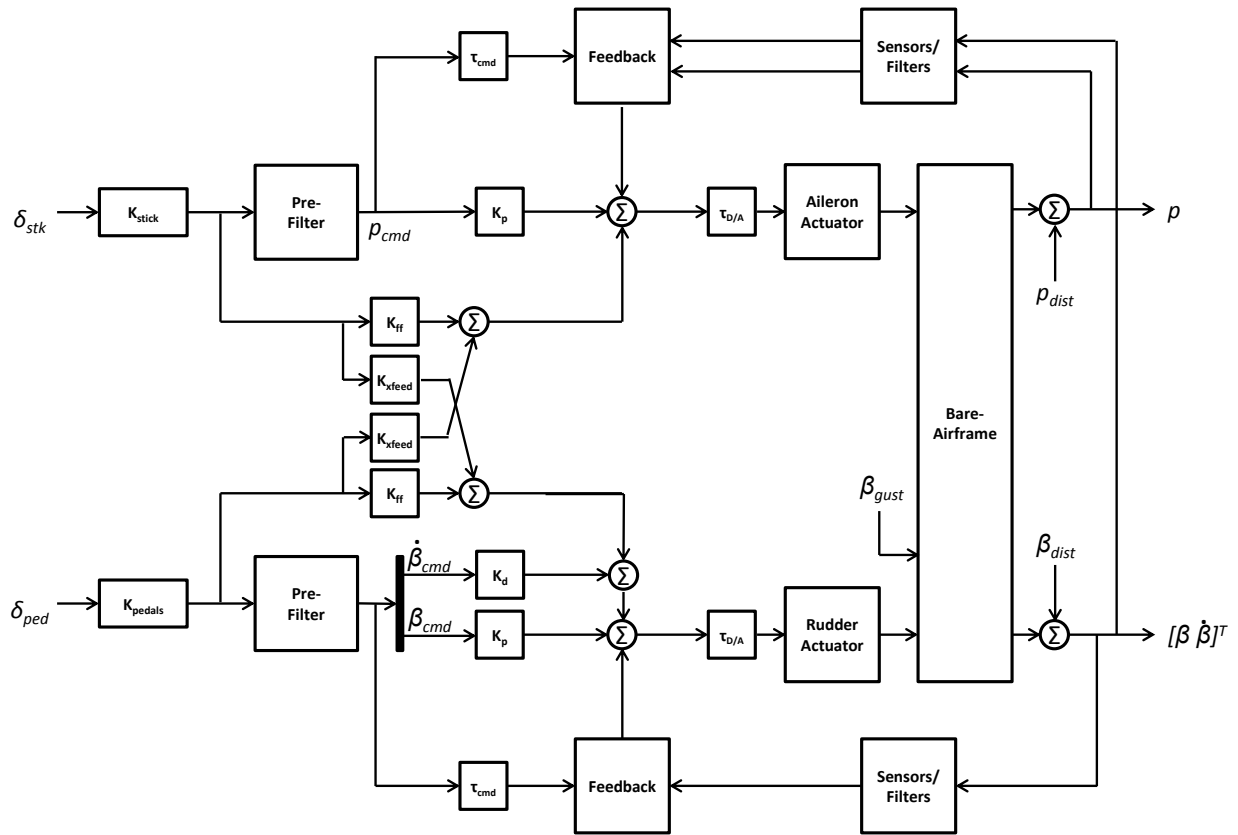


Figure 6. Schematic of lateral/directional control law block diagram.

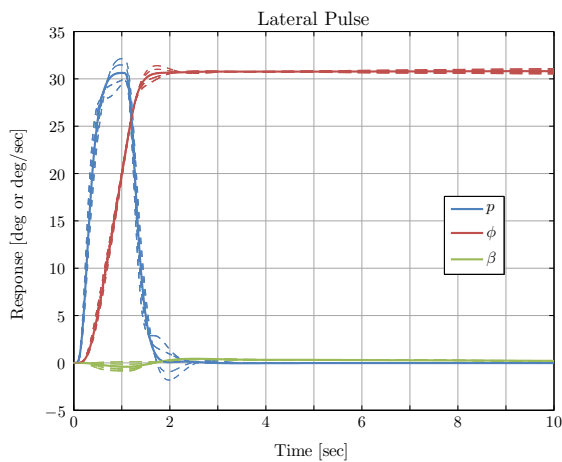


Figure 7. Time history response to a 1-second lateral stick input (Mach 0.3/5000 ft flight condition; All weight/CG configurations).

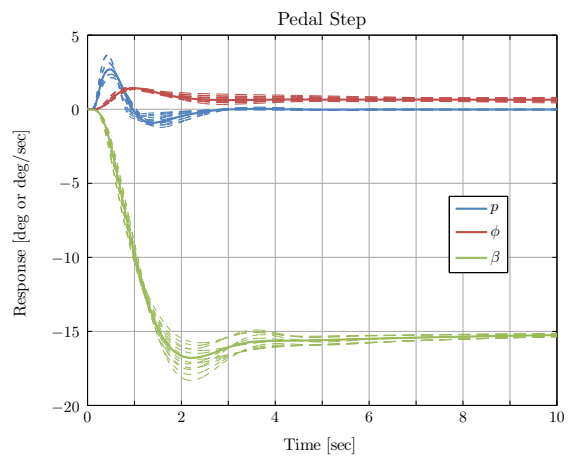


Figure 8. Time history pedal step response (Mach 0.3/5000 ft flight condition; All weight/CG configurations).

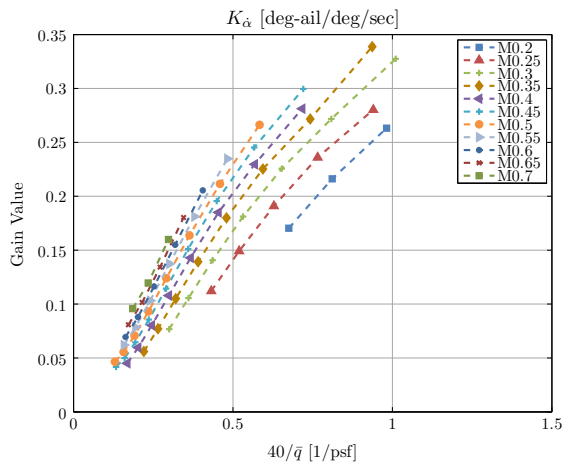


Figure 9. Example longitudinal feedback gain schedule.

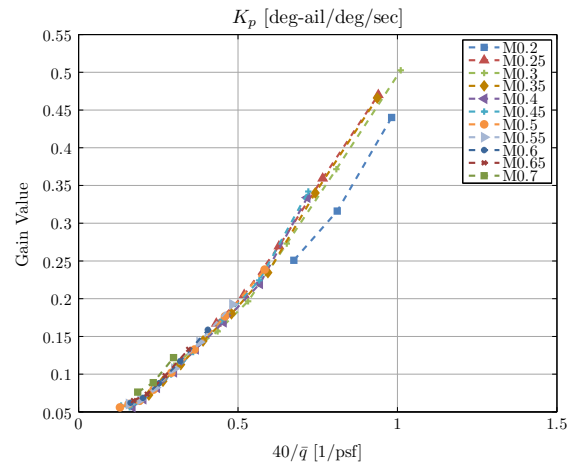


Figure 10. Example lateral/directional feedback gain schedule.

4. Trim Implementation

The control laws must command and feed back total (not perturbation) aircraft states, and generate total control surface commands. Therefore, lookup tables of trim aircraft states and control surface deflections must be included in the control laws. As shown in Figure 11 for the longitudinal axis, trim aircraft states (e.g. n_{z_0}) are summed with the perturbation commands (e.g. Δn_z) to command total aircraft states, which are compared with the total measured aircraft states (e.g. $n_{z_{tot}}$). Trim control surface deflections (δ_{elev_0}) are summed with the control law commands to generate total control surface deflection commands ($\delta_{elev_{tot}}$). This is done in preference to pre-loading the integrator in each axis with the trim control surface deflection in order to keep the contribution of the integral path small, and be able to limit its overall authority. Note that the trim states and control surface deflections are functions of Mach, dynamic pressure, and flap

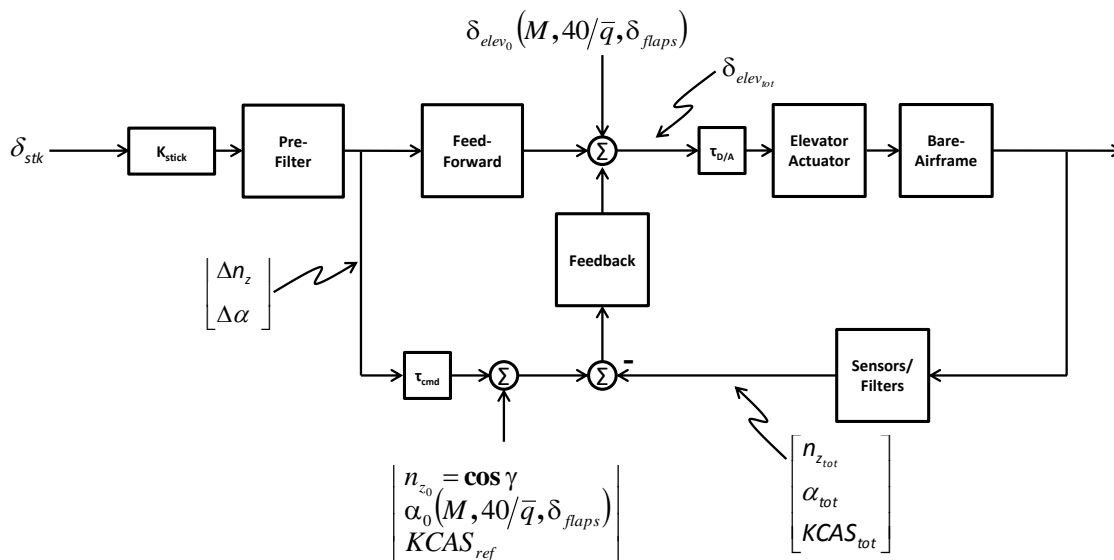


Figure 11. Block diagram schematic showing trim implementation.

5. Gain Scheduling Air Data Filter

As mentioned in Sections II.B.3 and II.B.4, the gain and trim schedule lookup tables are functions of Mach and dynamic pressure. Both the Mach and dynamic pressure signals are smoothed with a first-order, low-pass filter with a break frequency of 0.2 rad/sec for use in the control laws. Applying this filter ensures that the gains and trim values stay constant for short term motion, and do not follow, or chase, turbulence.

6. Reference Airspeed

The longitudinal $n_z u$ control laws require a reference airspeed in order to calculate the airspeed error u . This reference speed is given in knots of complimentary filtered calibrated airspeed (KCAS), and is controlled by the pilot via the pitch trim switch on the sidestick and displayed on the primary flight display (PFD).

The reference airspeed that the pilot can set is limited to:

$$1.3V_{MCA} \leq KCAS_{ref} \leq V_{MO} \quad (1)$$

where V_{MCA} is scheduled with flaps. In addition, the airspeed error is limited to ± 50 kts, which corresponds to a limit on the normal acceleration command of $\pm 1/6$ g.

7. Integrator Anti-Windup

As mentioned above, trim control surface commands are carried in a lookup table and summed with the output of the control system. Therefore, trim is not carried by the integral path, aside from small corrections to the values in the lookup table due to off-nominal conditions.

Several strategies are employed to avoid and mitigate integrator windup. The first is to limit the authority of the integral path to ensure that the forward command path and stabilizing rate feedback paths always have enough authority for command and stabilization of the aircraft. In the lateral and directional axes, the integrators are limited to $\pm 10\%$ authority of the full control system authority. In the longitudinal axis, the integral path provides speed stability, and is used to track the reference airspeed commanded by the pilot (as described in Section II.B.6). Therefore, the integrator is given a larger, $\pm 50\%$ authority.

The second strategy implemented to mitigate integrator windup is that in each axis, when either the integral path alone or the entire control system saturates, the signal to the integrator path is disabled until the error signal changes direction. This is a classical anti-windup logic.

8. Turn Coordination and Compensation

Turn coordination is provided automatically by the “ p - β ” lateral/directional control laws. For turn compensation, the longitudinal control laws include a pitch command to maintain altitude in a constant bank angle steady turn. Since the longitudinal control laws command stability axes normal acceleration, n_z , the normal acceleration required to maintain altitude during a steady turn:

$$n_{zTC} = \frac{\cos\gamma}{\cos\phi} \quad (2)$$

is added to the pilot’s normal acceleration command input. Note that the bank angle, ϕ , used to calculate n_{zTC} is limited to ± 33 deg.

9. Stick Force Per Knot For Flare

The flare characteristics of the control system were tuned in the simulator by modifying the stick force per knot gradient when the landing gear are deployed. The stick force per knot gain (set to 1/6 lb/kt for the normal mode control laws¹) was increased to 2/3 lb/kt for the flare mode. This increase requires the pilot to pull back more on the sidestick as the aircraft slows below its reference airspeed before touchdown. The stick force per knot gain was tuned to maintain stick motion similar to flaring the bare-airframe.

Based on lessons learned for the Boeing 777,¹⁶ further simulation would be needed to refine the stick force per knot gain for touchdown and derotation using high-gain tasks such as on-runway attitude tracking.

10. Lateral/Directional Off-Axis Feed-Forward Gain Tuning

The off-axis feed-forward gains in the control laws (K_{xfeed} in Figure 6) are used to tune the off-axis responses with no effect to the on-axis response,² however final tuning of these gains to ensure good handling qualities is generally done in piloted simulation. This was investigated during initial simulation checkout and pilots noted good lateral responses to pedal input, but larger than desired yaw rate excursions during lateral maneuvers such as banking the aircraft. In this case, it is the off-axis feed-forward gain from roll rate command to rudder (i.e. $K_{ff_p \rightarrow r_{rud}}$) that affects the yaw rate of the aircraft during lateral maneuvers. During design of the control laws, this gain was tuned to meet the proverse off-axis requirement for the sideslip response only.² In the simulator, this gain was adjusted to meet the requirement for the yaw rate response as well.

Figure 12 shows the aircraft response to a lateral stick pulse for the original gain value and the adjusted gain value. The on-axis roll rate and bank angle responses are unchanged. However, the sideslip and yaw rate excursions are reduced, as is the rudder deflection. In addition, the non-minimum phase yaw rate response is eliminated. The adjusted gain was tested at several different flight conditions in the simulator, and an updated gain schedule was developed.

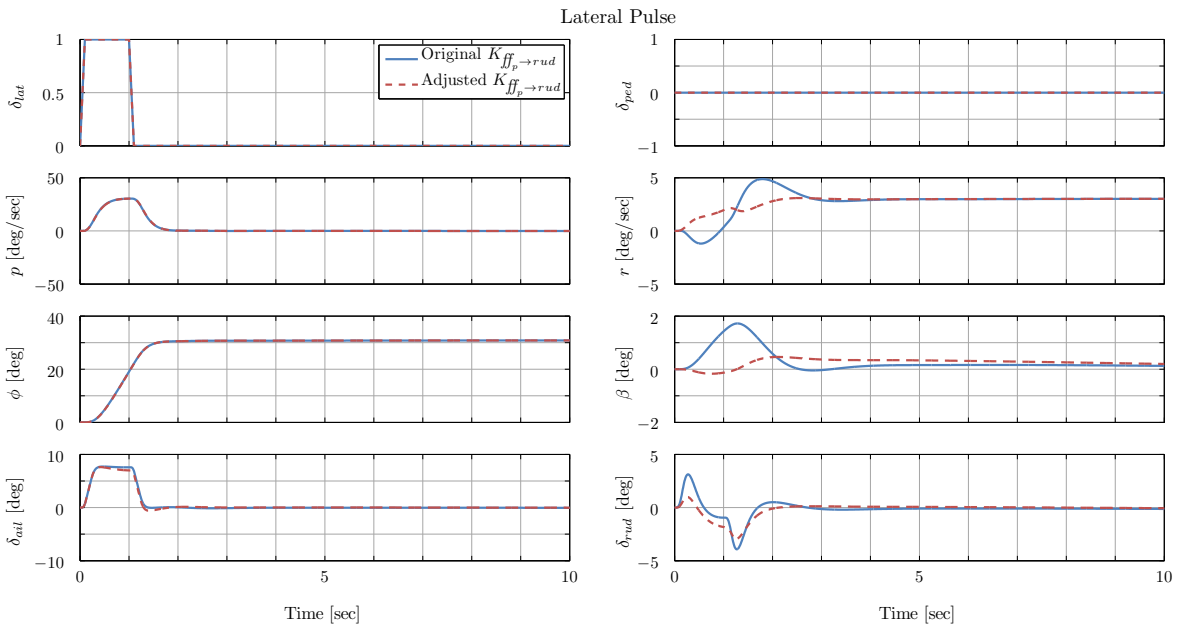


Figure 12. Lateral stick pulse response.

11. Sidestick Shaping

Shaping of the sidestick commands was tuned in the simulator. The maximum command was scheduled with KCAS for the pitch and yaw axes to limit the normal acceleration and sideslip commands. In the roll axis, the stick shaping was held constant with airspeed to provide a constant maximum roll rate command per sidestick deflection. In all axes, the maximum command was limited to stay within the bare-airframe's control power capability.

C. Bare-Airframe Configurations

To provide a comparison to the FBW control laws, the bare-airframe was also be tested. The bare-airframe was flown using traditional column and wheel with control loading. In addition, the bare-airframe model includes a yaw damper which is set to disengage at the autopilot minimum use height of 200 ft above ground level (AGL).

D. Modeled Disturbances

The aircraft simulation used in this experiment contains several commonly used disturbance models in order to assess the control laws in realistic atmospheric conditions. The Dryden turbulence model⁶ was used to simulate either ambient or moderate turbulence for all assessed tasks. In addition, during the landing tasks, a 1-cosine discrete angle-of-attack or sideslip gust was applied at about 200 ft AGL to induce the pilot to enter the control loop. The gusts were of the form:

$$\alpha, \beta_{gust} = \frac{K_g}{2} (1 - \cos(\omega_g t)), 0 \leq t \leq 2\pi/\omega_g \quad (3)$$

where,

$$K_g = \pm 10 \text{ deg for } \alpha_{gust} \text{ and } \pm 15 \text{ deg for } \beta_{gust}, \text{ and}$$

$$\omega_g = \omega_{sp} \text{ for } \alpha_{gust} \text{ and } \omega_{dr} \text{ for } \beta_{gust}.$$

III. Simulation Facility and Validation

This simulation experiment was conducted using the Cessna fixed-based business jet simulator. Figure 13 shows a picture of the simulation facility, which is based on a modified Cessna Citation Excel cab. The outside visual displays provide the pilot with a 170 deg field of view using commercially available LCD projectors. The inceptors in the cab consist of a commercially certified passive sidestick, shown in Figure 14, as well as rudder pedals with control loading and conventional throttles. Communications between the simulation model and the displays is accomplished via UDP packets updated at 200 Hz.



Figure 13. Cessna's fixed-based simulator.



Figure 14. Sidestick inceptor.

A. Time Delay Measurement and Correction

It is important to account for the time delay inherent in the simulator hardware, from such sources as the inceptor dynamics and filters, computational delay, and visual processing delay in the projectors. In this case, a measurement of the total, lumped delay (τ_{sim}) was made by configuring the model to make the outputted aircraft attitude proportional to stick position (with no dynamics or internal model delays). Then, high speed (60 frames per second) video of rapid stick pulses was recorded with the sidestick, visuals, and a stopwatch in the frame. The video was then advanced frame by frame, and the time difference between when the stick first moved to when the aircraft attitude in the visuals first moved was used to estimate the time delay within an error of plus or minus half a frame:

$$\tau_{sim} = 0.05 \pm 0.008 \text{ sec} \quad (4)$$

Not accounting for this additional delay could render a Level 1 control system to be rated Level 2 by the pilots. Therefore, to compensate for this simulation hardware delay, a total of 50 msec was removed from the forward path of the simulation model. This was done by removing the 5 Hz anti-aliasing stick filters (roughly 32 msec) which is implemented in the sidestick hardware and does not need to be accounted for in the model, as well as 10 msec computational delays and 10 msec digital-to-analog sample-and-hold delays. The anti-aliasing stick filters are in the feed-forward path of the control laws only, and not in the feedback path. Therefore, removing this filters has no affect on the control laws' feedback characteristics, such as stability margin or disturbance rejection bandwidth. However, the computational and sample-and-hold delays are in both the forward and feedback paths. Therefore, removing these delays from the forward path meant they had to be moved into the feedback path in order to not affect on the control laws' feedback characteristics. Section III.B shows a validation of this approach.

B. Model Validation

In order to validate the implementation of the nonlinear simulation model, dynamic checks were performed at a specific flight condition (Mach 0.3/5000 ft). This was done by conducting both closed-loop and broken-loop automated frequency sweeps. The frequency sweep simulation data were analyzed using CIFER[®]⁸ to extract the appropriate frequency responses and compare to those of the linear point model used in the control law development. Three responses were analyzed in each axis: the closed-loop piloted response comparison validates the implementation of the feed-forward and feedback sections of the control laws; the closed-loop disturbance response and broken-loop response comparisons validate the implementation of the stitched model and the feedback section of the control laws. This was also used as a way to validate the modifications made to the simulation model to account for the simulator hardware time delay, namely, removing the stick anti-aliasing filter and moving 20 msec of feed-forward path time delay to the feedback path, as explained in Section III.A.

Figures 15 through 17 show the closed-loop frequency responses, broken-loop (at the actuators) frequency responses, and disturbance frequency responses, respectively, in the longitudinal axis for both the nonlinear simulation model and linear analysis models. The figures show an excellent agreement between the simulation and linear models, validating the implementation of the stitched model, gain schedule, and control laws in the simulation model. Table 1 shows the pertinent control system metrics for all axes. Again, the excellent agreement between the simulation and analysis models indicates a proper implementation of the control laws.

Figure 18 shows a closed-loop time history comparisons between the simulation and linear analysis models. The time histories match very well, with small steady-state differences due to the simulation model moving away from the trim condition.

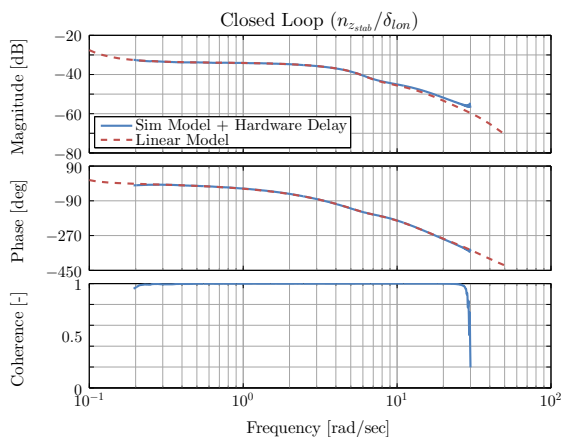


Figure 15. Closed-loop normal acceleration response.

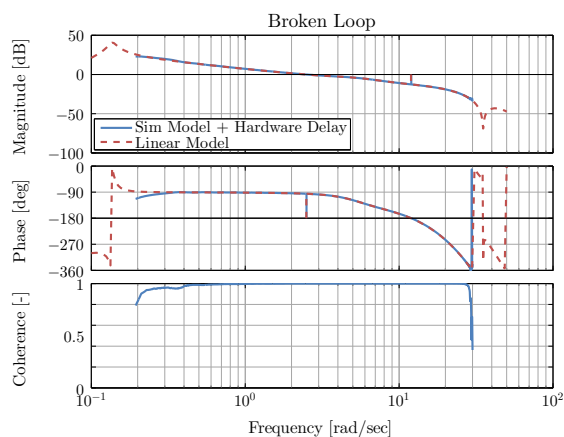


Figure 16. Longitudinal broken loop response.

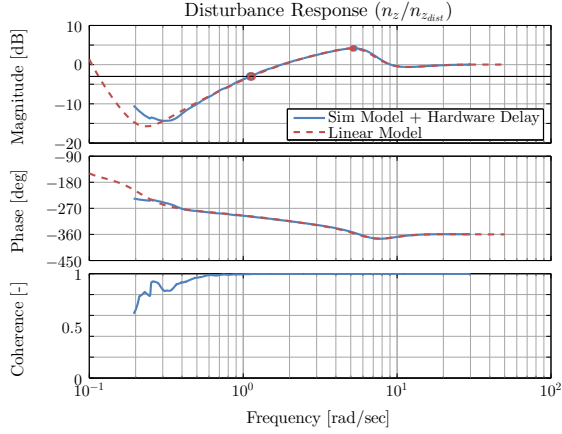


Figure 17. Normal acceleration disturbance response.

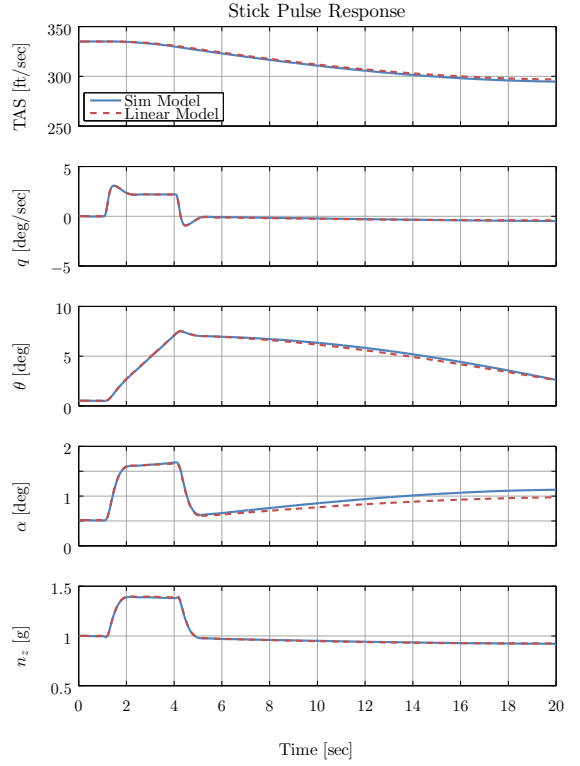


Figure 18. Longitudinal stick pulse response.

Table 1. Simulation and Linear Point Model Comparison

Axis Model	Longitudinal		Lateral		Directional	
	Sim Model	Linear Model	Sim Model	Linear Model	Sim Model	Linear Model
ω_{BW_g} [rad/sec] [*]	5.07	5.06	3.51	3.56	3.89	3.87
ω_{BW_p} [rad/sec] [*]	4.29	4.33	2.49	2.49	2.7	2.72
τ_p [sec] [*]	0.09	0.08	0.09	0.09	0.09	0.09
ω_c [rad/sec] [†]	2.50	2.50	3.50	3.50	3.50	3.50
PM [deg] [†]	81.44	81.42	52.61	52.61	74.88	74.89
GM [dB] [†]	12.40	12.35	11.26	11.24	12.34	12.31
DRB [rad/sec] [‡]	1.18	1.19	1.69	1.69	0.29	0.29
DRP [dB] [‡]	4.11	4.13	4.20	4.20	1.20	1.19

^{*}Attitude bandwidth (θ , ϕ , and ψ , respectively)

[†]Loop broken at actuator (elevator, aileron, and rudder, respectively)

[‡]Disturbance response ($n_z/n_{z_{dist}}$, $\int p/\int p_{dist}$, and β/β_{dist} , respectively)

IV. Experimental Setup

A. Handling Qualities Task Definition

Handling qualities tasks were selected from MIL-STD-1797B⁶ as well as an Air Force handling qualities demonstration maneuver catalog⁷ and FAA advisory material.¹⁷ Tasks were selected to be operationally relevant for a business jet (e.g. landing, offset landing, and capture tasks), but also be high-gain (e.g. attitude tracking tasks) to detect possible handling qualities “cliffs.”

1. Pitch and Roll Capture

Pitch and roll capture tasks were used to evaluate the handling qualities for gross acquisition. As stated in MIL-STD-1797B,⁶ these tasks are usually done “almost precognitively by the pilot” and are “usually over so quickly that they do not lend themselves well to use with the [Cooper-Harper HQR] scale.” Therefore, desired and adequate performance bounds were not used for these tasks. Instead, pilots were asked to acquire the target attitudes as closely as possible, at a rate they would find aggressive for a business jet.

For the pitch capture task, pilots were instructed to start at trim, level flight, pitch up to a pitch attitude of $\theta = 5$ deg, pitch down to a pitch attitude of $\theta = -5$ deg, and finally pitch back up to trim, level flight. For the roll capture task, pilots were instructed to start at trim, level flight, roll right to a bank angle of $\phi = 20$ deg, roll left to a bank angle of $\phi = -20$ deg, and finally roll back right to trim, level flight.

2. Pitch and Roll Tracking

Pitch and roll tracking tasks were used to evaluate continuous closed-loop controllability in a high pilot gain task. For this task, a target symbol (the flight director) was displayed which commanded pitch or roll changes that the evaluation pilot was instructed to follow. The pitch and roll commands were generated using a randomized sum-of-sines, as illustrated for an example record in Figure 19. Using the known forcing function for the tracking task, elements of the pilot-vehicle system can be identified, in order to assess the pilot-vehicle open-loop crossover frequency and a describing function of the pilot. These analyses enable calibrating the pilots’ gains and correlating piloting metrics with the handling qualities design criteria.

The pitch and roll sum-of-sines tracking signals and performance criteria were designed based on guidance from the Air Force Handling Qualities Demonstration Maneuver Catalog,⁷ with some modifications to account for the class of aircraft being tested here (i.e., a business jet, not a fighter). The sum-of-sines signal was designed using a Fibonacci-based sequence based on the length of the score time, which ensures that the scored data includes at least one full cycle of each sinewave and that there is an integer number of all sinewaves. The scoring time in this case is 60 sec, preceded by a 5 sec ramp-in time and 5 sec settle time, and followed by a 5 sec ramp-out time. The phasing of the sinewaves was randomized for each run to make sure the pilots saw a different signal each time.

Figure 20 shows the power spectral density of the sinewaves. The magnitudes of the higher frequency sinewaves are intentionally reduced to provide the signal a bandwidth of roughly 1.5 rad/sec.⁷ Additionally, the magnitudes of the target signals were scaled to give the signals an overall root mean square (RMS) of about 2.5 deg in pitch and 6 deg in roll.

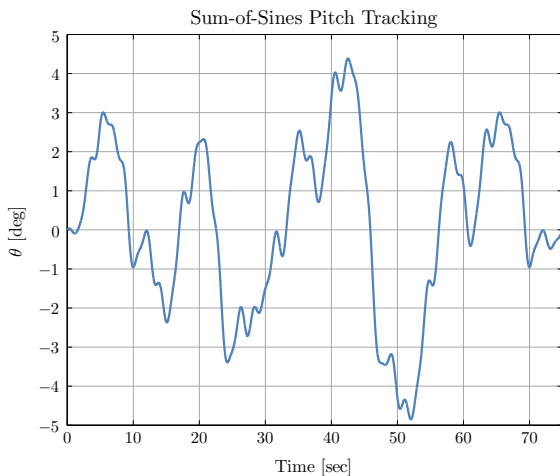


Figure 19. Example sum-of-sines pitch attitude tracking sequence.

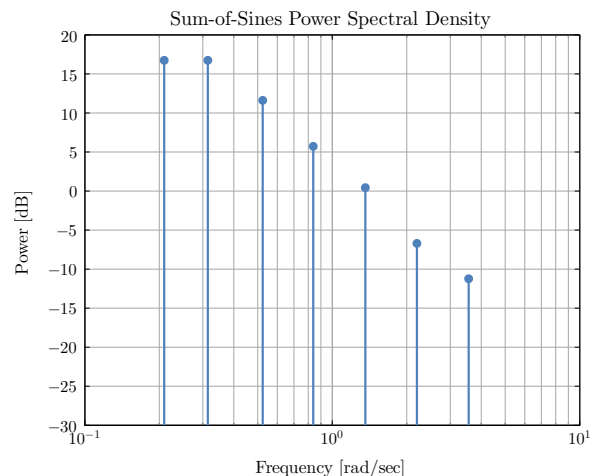


Figure 20. Sum-of-sines pitch attitude tracking sequence power spectral density.

For the pitch tracking task, performance criteria were taken from the Air Force Handling Qualities Demonstration Maneuver Catalog⁷ and are shown in Table 2. In the case of the roll tracking task, the performance criteria, also shown in Table 2, were modified to align with the flight director display in the simulator.

Table 2. Performance Criteria - Tracking

	Desired	Adequate
<i>Pitch*</i>		
Remain within 10 mils [†] for X percent of the time	50 %	-
Remain within 20 mils for X percent of the time	-	50 %
No PIO	✓	✓
<i>Roll[‡]</i>		
Remain within 3.5 deg for X percent of the time	50 %	-
Remain within 7.0 deg for X percent of the time	-	50 %
No PIO	✓	✓

*Pitch performance standards from Air Force Handling Qualities Demonstration Maneuver Catalog⁷

[†]1 mil = 0.057 deg

[‡]Roll performance standards modified to fit available display

3. Precision and Offset Precision Landing

Since the offset landing task exercises both the pitch and roll axes, a landing task with no offset was also used to isolate the pitch axis. Both tasks were flown in two levels of turbulence—ambient and moderate. In addition, the landing task with no offset included a vertical gust while the landing task with an offset included a lateral gust. The gusts, of the form shown in Equation 3 in Section II.D, were applied at about 200 ft AGL, with the magnitudes of the gusts kept constant between runs, but the directions randomized.

Both landing tasks are divided into two phases—approach and touchdown. The approach phase evaluates the ability to control flightpath, airspeed, and attitude. The approach phase began three miles out on final approach, with gear and flaps down at the required glideslope angle, but with a lateral offset from the runway centerline of 300 ft (for the lateral offset landing task only). The pilots maintained precise flightpath angle and airspeed control throughout the approach phase, and were aligned with the left side of the parallel taxiway for the case with offset, up to the offset correction point at 200 ft AGL. The touchdown phase evaluates the ability to control airspeed, sink rate, and attitude to a precise touchdown, and began at about 50 ft AGL. The pilots attempted to land with the main wheels inside a designated touchdown zone at a specified sink rate. Figure 21 shows the offset landing task and performance metrics. Table 3 lists detailed desired and adequate performance objectives for the tasks.

Table 3. Performance Criteria - Offset Landing

	Desired	Adequate
<i>Approach</i>		
Remain within X degrees of glideslope angle	±1 deg	±2 deg
Remain within X kts of approach speed	±5 kts	±10 kts
No PIO	✓	NA
<i>Flare/Touchdown</i>		
Within X ft of aim point laterally	±10 ft	±27 ft
Within X ft of aim point longitudinally	-75 to +425 ft	-325 to +1175 ft
Within X kts of approach speed at flare initiation	±5 kts	±10 kts
Less than X ft/sec sink rate at touchdown	≤ 4 ft/sec	≤ 7 ft/sec
No PIO	✓	NA

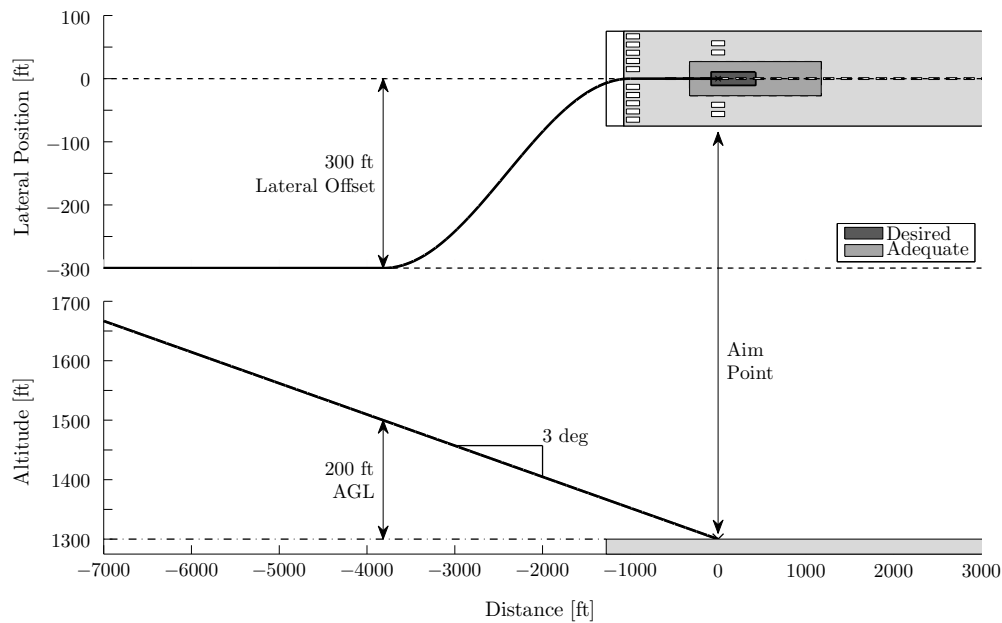


Figure 21. Offset landing task and performance metrics.

B. Data Collection and Procedures

Pilots completed initial training sessions to familiarize themselves with the aircraft flight dynamics, the control system, the tasks, and the particulars of the visual cueing provided in the simulator. Prior to evaluation runs, the pilots flew each configuration for practice purposes as many times as required until they felt consistent performance could be achieved. For the formal evaluation runs, pilots performed a minimum of three runs prior to collection of pilot comments and ratings. Pilots were allowed to execute additional runs if they felt one of the data runs was anomalous or if they needed additional runs to fully evaluate the configuration. Following each run, task performance information was read back to the pilot to assess compliance with the task desired and adequate performance standards.

Data collected during the experiment included all aircraft state and control data, simulated wind and turbulence levels, task performance metrics, as well as pilot comments and ratings. Pilots answered the questionnaire provided in Appendix A. At the end of the questionnaire, pilots used the Cooper-Harper Handling Qualities Rating (HQR) Scale,¹⁸ shown in Figure 59 in Appendix A, as well as the PIO rating scale¹⁹ if unacceptable oscillations were present. These qualitative data were used along with the quantitative data collected to correlate the control system’s assessed handling qualities with its predicted handling qualities.

C. Matrix of Configurations

Three test pilots conducted handling qualities evaluations for this experiment. Two of the pilots are Cessna engineering test pilots very familiar with small business jets similar to the one used in this experiment. The third pilot is a U.S. Army experimental test pilot.

The full test matrix is shown in Table 7 in Appendix B. The initial goal was to have each of the three test pilots complete the full test matrix. However, for the tracking tasks, several of the off-nominal loading configurations were not tested with all pilots as the pilots who did test them could not tell the difference between, and had almost identical performance for, the nominal and off-nominal loading configurations.

The off-nominal loading configuration for each task was chosen based on which ever loading configuration has the minimum damping ratio at the flight condition and primary axis of each task. Table 4 shows which off-nominal configuration was used for each task.

Table 4. Off-Nominal Configurations

Task	Flight Condition	Off-Nominal Configuration (Weight/CG Location)
Pitch Capture	M0.3/5000 ft	Light/Aft
Pitch Capture	M0.58/FL350	Heavy/Fwd
Roll Capture	M0.3/5000 ft	Heavy/Aft
Roll Capture	M0.58/FL350	Heavy/Aft
Pitch Tracking	M0.3/5000 ft	Light/Aft
Pitch Tracking	M0.58/FL350	Heavy/Fwd
Roll Tracking	M0.3/5000 ft	Heavy/Aft
Roll Tracking	M0.58/FL350	Heavy/Aft
Precision Landing	Approach	Light/Aft
Lateral Offset Precision Landing	Approach	Heavy/Aft

V. Results

A. Pitch Capture

Pilots reported that the pitch capture task was “fairly easy” to achieve, and that the response was “predictable” and with “no oscillations.” In addition, the pilots noted that they could be “quite aggressive” with “very high precision.” Pilots did note the dropback characteristic of the pitch attitude response, however, this was not objectionable and since it was predictable, the pilots could easily compensate for it by overshooting the desired attitude and allowing the aircraft to drop back to it.

Figure 22 shows the pitch attitude dropback of the different flight conditions and loading configurations tested. The empty symbols are calculated from the simulation data, an example of which is shown in Figure 23. The filled in symbols are from the analysis model.¹ There is a bit of a spread in the points in Figure 22 because the pilots sometimes shaped their inputs differently to try different capture strategies. However, the points all lie within the Level 1 region of the specification, and show consistent trends with the analysis model. Namely, that the Mach 0.58/FL350 condition has slightly higher dropback than the Mach 0.3/5000 ft flight condition, and that at each flight condition, the difference between the dropback of the different loading configurations is small. This second point was corroborated by the pilots who commented that there was no noticeable difference between the different loading configurations at each flight condition when performing the pitch capture task.

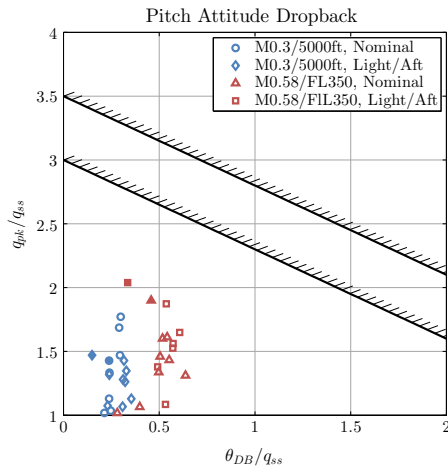


Figure 22. Pitch attitude dropback of all pitch capture runs.

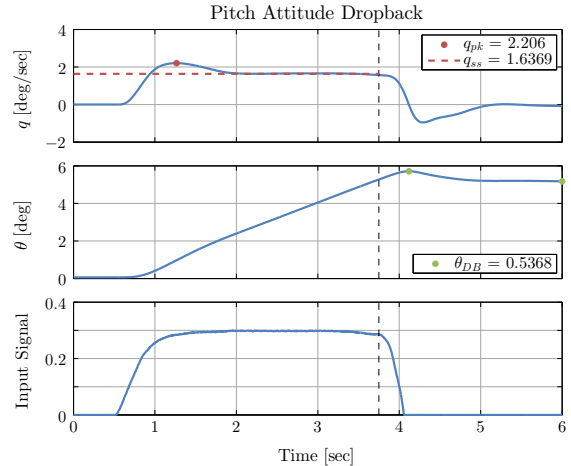


Figure 23. Example pitch attitude dropback calculation using one pitch capture run.

As expected, when performing the task at the Mach 0.58/FL350 flight condition, the pilots were less aggressive than at the Mach 0.3/5000 ft flight condition, in order to maintain similar peak normal accelerations during the maneuver.

B. Roll Capture

For the roll capture task, pilots were able to precisely acquire the desired bank angle targets. They commented that the aircraft response was “predictable,” “linear,” and with no oscillations or overshoots. At the Mach 0.3/5000 ft flight condition, pilots noted no difference between the nominal and off-nominal loading configurations. At the Mach 0.58/FL350 flight condition, two of the three pilots noted no difference between the nominal and off-nominal loading configurations, while one pilot noted that the roll rate for the heavy-weight/aft-CG configuration would return to zero a little slower when returning the stick to detent, and this would result in an additional 1-2 deg of bank angle.

Figure 24 shows the sideslip excursions of the different flight conditions and loading configurations tested. The empty symbols are calculated from the simulation data, an example of which is shown in Figure 25, while the filled in symbols are from the analysis model.² As with the pitch capture task above, there is a spread in the simulation data due to the pilots using different levels of aggressiveness or different shaped inputs, however, all the results are in the Level 1 region. The spread in the simulation data is mainly manifested in the phasing of the Dutch roll oscillations in the roll rate and sideline responses, ψ_β . Numerically extracting this parameter is sensitive to finding oscillations in the roll rate and sideslip responses. However, as shown in Figure 25, no Dutch roll oscillations are present in the roll rate response, due to the good design of the lateral/directional cross-feed gains,² and so the phasing angle, ψ_β , is sensitive to small bumps in the roll rate response. The sideslip excursion parameter, $\Delta\beta/k$, is not as sensitive because it is scaled by the magnitude of the bank angle response, and has good agreement between the simulation data and analysis model.

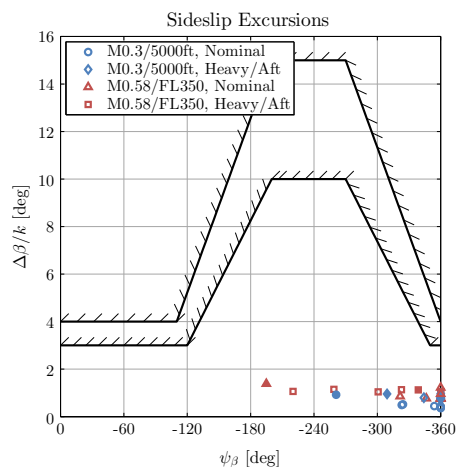


Figure 24. Sideslip excursions of all roll capture runs.

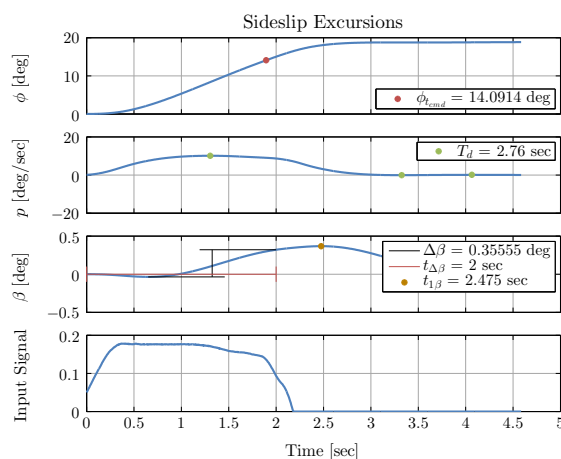


Figure 25. Example sideslip excursion calculation using one roll capture run.

C. Pitch Tracking

Figure 26 shows the pilot HQRs for the pitch tracking task at each flight condition and loading configuration combination. Figure 27 shows the pilot task performance for each configuration tested. The performance is shown in terms of percent time spent within ± 10 mils of the target signal, with over 50% being desired performance (as described in Section IV.A.2). The points on Figure 27 are the average performance for all of a pilot’s data runs, while the errorbars show the best and worst performance. The ratings and performance are all flat with different flight conditions and loading configurations, showing good robustness of the control laws to changes in aircraft loading and consistent performance of the gain schedule across the flight envelope.

The HQRs for pitch tracking were largely task driven. All pilots agreed that this task was too aggressive and not representative of an actual maneuver an aircraft of this class would perform, although understood that the purpose of the task was to exercise the control system in a high-gain pilot-in-the-loop fashion.

Pilot A was able to meet desired performance and be aggressive with good precision, and therefore assigned all Level 1 HQRs for this task. Furthermore, even with large, almost stop-to-stop control inputs there were no unacceptable oscillations or tendencies to PIO.

Pilot B's strategy was to go slow, flying the aircraft in a more business jet-like fashion, and attempting to meet adequate performance instead of desired. Since Pilot B averaged adequate performance, his rating for this task was an HQR 5. As performance and ratings were flat between loading configurations for both Pilots A and C, Pilot B did not repeat this task for the off-nominal loading configurations.

Pilot C was able to meet desired performance, however with moderate compensation, and therefore rated the task HQR 4. Pilot C did note that the required moderate compensation was task driven, and not prompted by the handling qualities of the aircraft, commenting that the handling was "very predictable" and that he could be very aggressive and precise. At both flight conditions, Pilot C commented that there were no noticeable differences between the nominal and the off-nominal loading configurations.

Figure 28 shows the actuator rate RMS and peak values during the pitch tracking tasks, and Figure 29 shows the actuator rate time histories for one of the pitch tracking runs at the Mach 0.58/FL350 flight condition and heavy-weight/aft-CG loading configuration. The actuator rates seen for this aggressive task are well within rate limits for standard hydraulic actuators with the loads seen at these flight conditions, and the lack of actuator rate limiting correlates well with the Level 1 Open Loop Onset Point (OLOP) criterion used in the control law design.¹

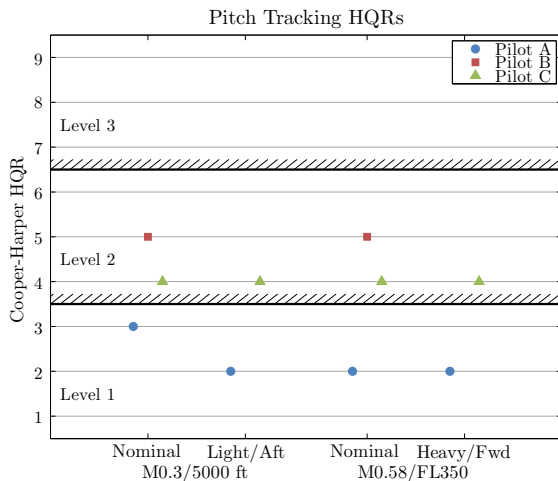


Figure 26. Pitch tracking HQRs.

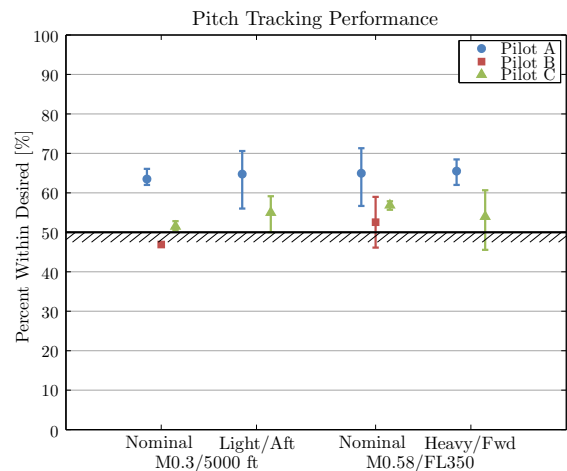


Figure 27. Pitch tracking task performance.

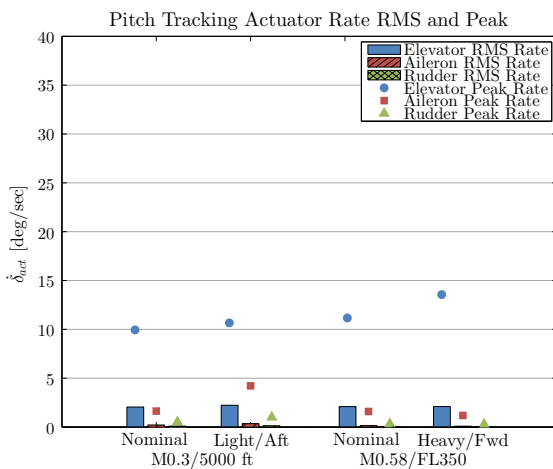


Figure 28. Actuator rate RMS and peak values during pitch tracking tasks.

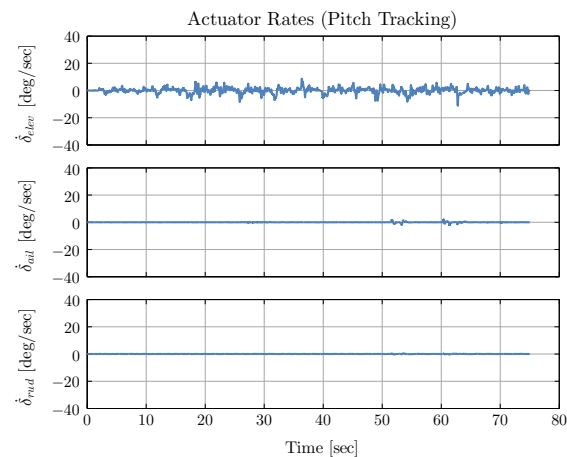


Figure 29. Example actuator rates during pitch tracking (M0.58/FL350, Heavy/Fwd).

1. Pilot Comparison

Quantitative task data, as shown for example in Figure 30, were used to calculate pilot-vehicle crossover frequencies as well as pilot cutoff frequencies, which correlate well with pilot performance and HQRs given for this task. The analysis and correlations are shown for the nominal loading configuration at the Mach 0.3/5000 ft flight condition only, but similar results were seen for all loading configuration and flight condition combination.

The pilot-vehicle crossover frequency (ω_c) is defined as the frequency at which the pilot-vehicle system (PVS) open-loop response crosses the 0 dB line, or:

$$Y_p Y_c = \frac{\omega_c}{s} e^{-\tau s} \quad (5)$$

Where,

Y_p denotes the pilot response ($\delta_{stk}/\theta_{err}$),

Y_c denotes the aircraft response (θ/δ_{stk}),

ω_c is the crossover frequency, and

τ is the equivalent time delay.

The crossover frequency is interpreted as the fundamental frequency of piloted control inputs for closed-loop regulation.⁸

The pilot cutoff frequency (ω_{co}) is defined as the half-power frequency of the pilot stick signal (δ_{stk}) determined via spectral analysis, and is a measure of the pilot's operating frequency. The cutoff frequency is a good estimate of the pilot-vehicle crossover frequency,^{8,20} especially useful when the error signal around which the pilot closes the loop is not available. In this case, where the error signal is known, both the crossover and cutoff frequencies were evaluated and compared to validate this approximation.

For this sum-of-sines pitch tracking task, the target signal had a bandwidth equal to about 1.5 rad/sec (Section IV.A.2), which sets the task bandwidth (ω_T).²¹ In the ideal case, to complete the task with desired performance the PVS crossover frequency will approximately equal the task bandwidth (i.e. $\omega_c \approx \omega_T$). However this does not account for unmodeled effects such as pilot remnant, and therefore in general, to achieve desired performance the real PVS crossover frequency will be greater than the task bandwidth ($\omega_c > \omega_T$).²² At the same time, the aircraft bandwidth (ω_{BW}) represents the maximum frequency at which a pure gain pilot closing the loop around the aircraft can operate without destabilizing the system, thus setting an upper limit on the PVS crossover frequency for minimal workload ($\omega_c < \omega_{BW}$).²²

Figure 31 shows the PVS ($Y_p Y_c$) describing function evaluated at the discrete sum-of-sines frequencies for the three pilots, as well as the crossover model (Equation 5) matched to each pilot and the pilot cutoff frequencies. Figure 32 shows the pilot (Y_p) describing functions for the three pilots, which has a flat magnitude response at the sum-of-sines frequencies of the target signal, indicating the pilots were operating in a pure-gain fashion ($Y_p = K_p e^{-\tau_p s}$) to complete the task. Table 5 lists the parameters of the open-loop PVS, as well as the simple pilot model matched to each pilots' describing function around crossover.

The PVS crossover frequencies, pilot cutoff frequencies, and pilot model gains are all consistent with the task performance each pilot achieved (Figure 27). Pilot A, who had the best task performance also has the highest pilot gain, and therefore the highest crossover and cutoff frequencies in excess of the sum-of-sines signal bandwidth, $\omega_c > \omega_T$. Pilot B had the lowest gain, with $\omega_c \approx \omega_T$, consistent with not meeting desired performance. Finally, for Pilot C who met desired performance, $\omega_c > \omega_T$. For all three pilots, the pilot cutoff frequency ω_{co} tracks the PVS crossover frequency ω_c well, though the absolute values differ for this aggressive task.

Figure 33 shows the aircraft pitch attitude response (Y_c) for the three pilots, evaluated at the discrete sum-of-sines frequencies, as well as the linear model pitch attitude response. For the model following control laws used here, the pitch attitude bandwidth of the aircraft is set by the second-order command model frequency.¹ Using the design approach of setting the command model frequency to match the bare-airframe's short period frequency, ω_{sp} , resulted in pitch attitude bandwidth values well above the minimum pitch attitude bandwidth requirement of $\omega_{BW} \geq 1.25$ rad/sec.⁶ For this flight condition for example, the installed aircraft pitch attitude bandwidth is $\omega_{BW} = 4.33$ rad/sec, which is well in excess of the PVS crossover frequencies. This allowed the pilots to operate in a pure-gains fashion (with no need for the pilot to generate any lead compensation) at frequencies above the task bandwidth ω_T , maintaining sufficient gain and phase margins (Table 5) and achieving desired performance.

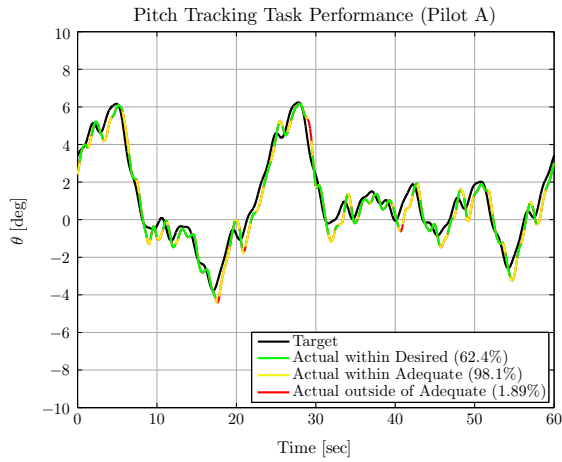


Figure 30. Example pitch tracking performance (Pilot A).

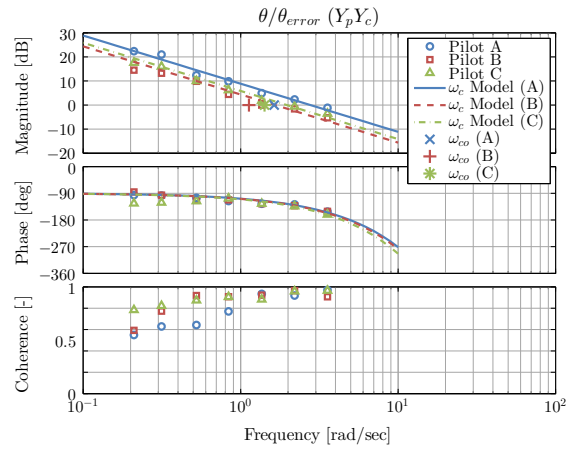


Figure 31. Pitch tracking pilot-vehicle describing function variations (M0.3/5000 ft, Nominal loading configuration, Pilots A-C).

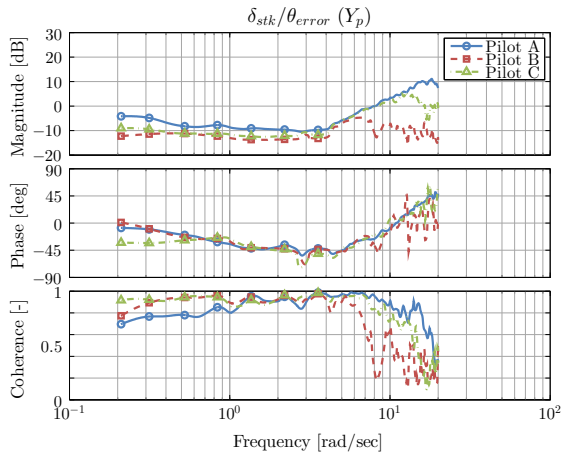


Figure 32. Pitch tracking pilot describing function variations (M0.3/5000 ft, Nominal loading configuration, Pilots A-C).

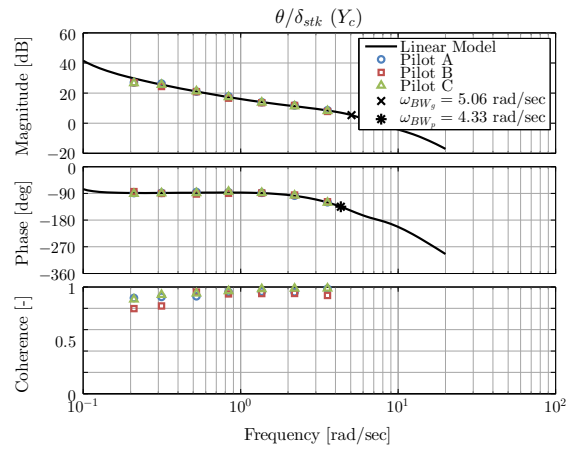


Figure 33. Pitch tracking vehicle describing function variations (M0.3/5000 ft, Nominal loading configuration, Pilots A-C).

Table 5. Pilot-Vehicle Parameters for Pitch Tracking Task

	Pilot A	Pilot B	Pilot C
<i>Pilot-Vehicle System Parameters (Y_pY_c)</i>			
Crossover Frequency ω_c [rad/sec]	2.77	1.66	1.96
Equivalent Time Delay τ [sec]	0.32	0.33	0.36
Gain Margin [dB]	5.04	9.21	7.04
Phase Margin [deg]	39.57	58.82	49.94
<i>Pilot Parameters (Y_p)</i>			
Cutoff Frequency ω_{co} [rad/sec]	1.63	1.13	1.42
Pilot Gain K_p	0.36	0.22	0.26
Time Delay τ_p [sec]	0.28	0.31	0.33

2. Loading Configuration Comparison

Pilots who tested both nominal and off-nominal loading configurations using the pitch tracking task could not tell the difference between configurations. This was the case both at the Mach 0.3/5000 ft and the Mach 0.58/FL350 flight condition. The similarity between nominal and off-nominal configurations can be seen by the similar HQRs given (Figure 26) and similar task performance (Figure 27). It can also be seen by comparing the PVS open-loop system and pilot describing function for the two loading configuration.

Figures 34 and 35 show a comparison of the PVS open-loop system and pilot describing function, respectively, for both the nominal and light-weight/aft-CG loading configurations for Pilot A at the Mach 0.3/5000 ft. The open-loop crossover frequency (ω_c), pilot cutoff frequency (ω_{co}), and pilot gain are nearly identical between the nominal and light-weight/aft-CG configuration. These similarities demonstrates the control laws' robustness to different loading configurations.

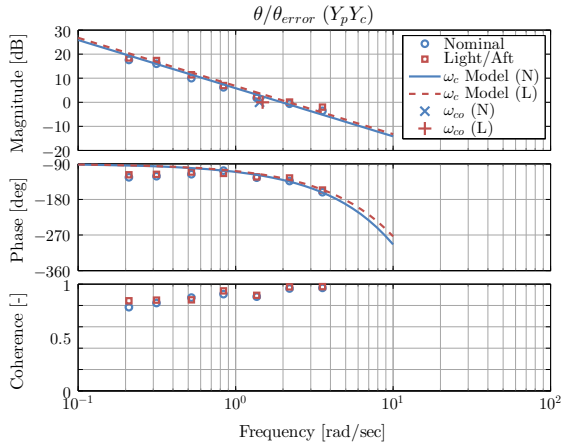


Figure 34. Pilot-vehicle describing function variations between loading configurations (Pilot C).

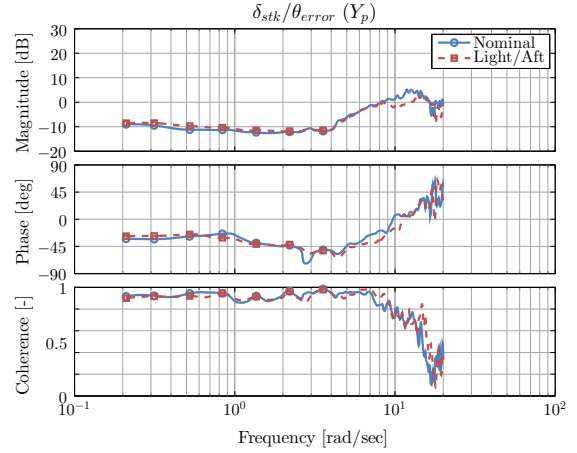


Figure 35. Pilot describing function variations between loading configurations (Pilot C).

D. Roll Tracking

Figures 36 and 37 show the pilot HQRs and task performance, respectively, for the roll tracking task at each flight condition and loading configuration combination. The performance is shown in terms of percent time spent within ± 3.5 deg of the target signal, with desired performance defined as over 50% time (Section IV.A.2). As with the pitch tracking results, the points on Figure 37 are the average performance for all of a pilot's data runs, while the errorbars show the best and worst performance. Similar to the results for the pitch tracking task, the ratings and performance for roll tracking are all flat with different flight conditions and loading configurations, showing good robustness of the control laws to changes in aircraft loading and consistent performance of the gain schedule across the flight envelope.

Unlike the pitch tracking task, pilots had an easier time meeting desired performance for the roll tracking task, with its wider performance bounds due to the display used. Therefore, all of the HQRs given for this task are Level 1. Pilot A commented that he was able to meet desired performance and that the task was not "particularly aggressive" although the ability to be was there. For both flight conditions, Pilot A noted no differences between the two different loading configurations tested.

Pilot B had similar comments, noting he could be aggressive when the target moved quickly, with no oscillations or overshoots, and that there was no difference between loading configurations.

Pilot C noted that this task was much better suited for a business jet type aircraft, whereas the pitch tracking task was more suited for a fighter type aircraft. Pilot C could be aggressive when necessary, and maintain good precision. Pilot C noted that there were no differences between the task at the different flight conditions or loading configurations, and that he could complete the task with "normal [piloting] techniques" and "minimal pilot compensation."

Figure 38 shows the actuator rate RMS and peak values during the roll tracking tasks, and Figure 39 shows actuator rate time histories for one of the roll tracking runs at the Mach 0.3/5000 ft flight condition and nominal loading configuration. The actuator rates seen for this task are well within rate limits for

standard hydraulic actuators with the loads seen at these flight conditions, and the lack of actuator rate limiting correlates well with the Level 1 OLOP criterion used in the control law design.²

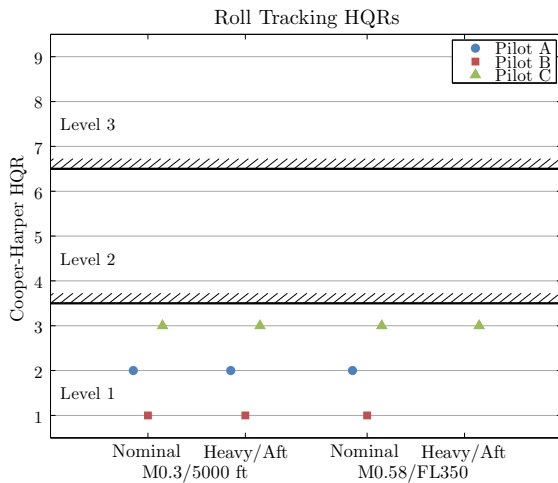


Figure 36. Roll tracking HQRs.

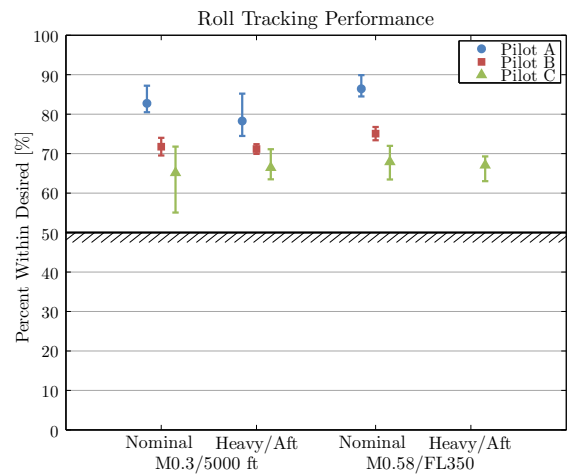


Figure 37. Roll tracking task performance.

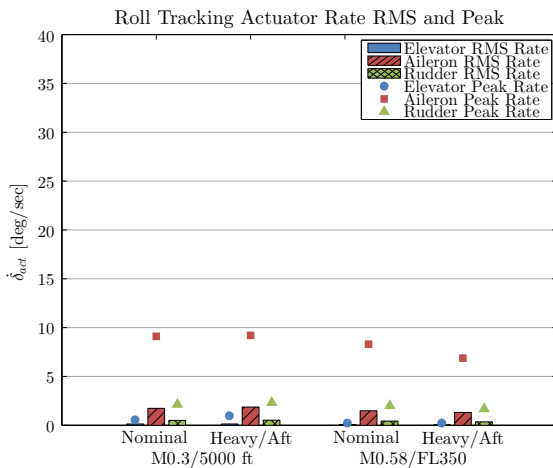


Figure 38. Actuator rate RMS and peak values during roll tracking tasks.

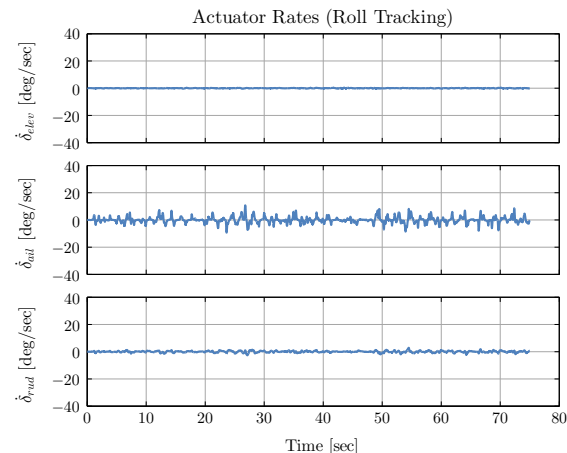


Figure 39. Example actuator rates during roll tracking (M0.3/5000 ft, Nominal).

1. Pilot Comparison

As with the pitch tracking task, quantitative task data, as shown for example in Figure 40, were used to calculate PVS crossover frequencies as well as pilot cutoff frequencies, which correlate well with pilot performance and HQRs given for this task. The analysis and correlations are shown for the nominal loading configuration at the Mach 0.3/5000 ft flight condition only, but similar results were seen for each loading configuration and flight condition combination.

Figure 41 shows the PVS ($Y_p Y_c$) describing function evaluated at the discrete sum-of-sines frequencies, for the three pilots, as well as the crossover model (Equation 5) matched to each pilot and the pilot cutoff frequencies. The parameters of the open-loop PVS are given in Table 7. Figure 42 shows the pilot describing functions for the three pilots, and Table 7 lists the parameters of the simple pilot model ($Y_p = K_p e^{-\tau_p s}$) matched to each pilots' describing function around crossover.

As with the pitch tracking task, the PVS crossover frequencies, pilot cutoff frequencies, and pilot model gains are all consistent with the task performance each pilot achieved shown in Figure 37. Consistent with pilots commenting that the roll tracking task was easier than the pitch tracking task, the pilots were operating

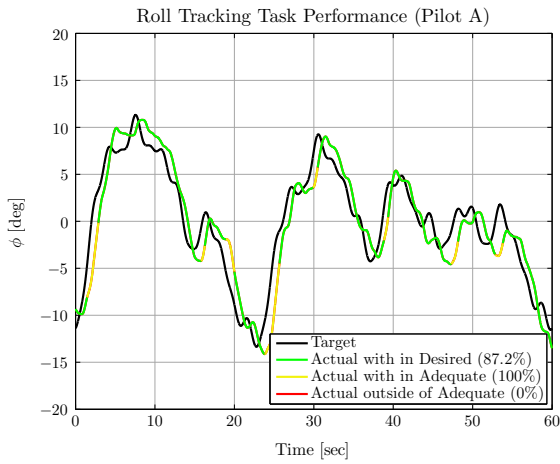


Figure 40. Example roll tracking performance (Pilot A).

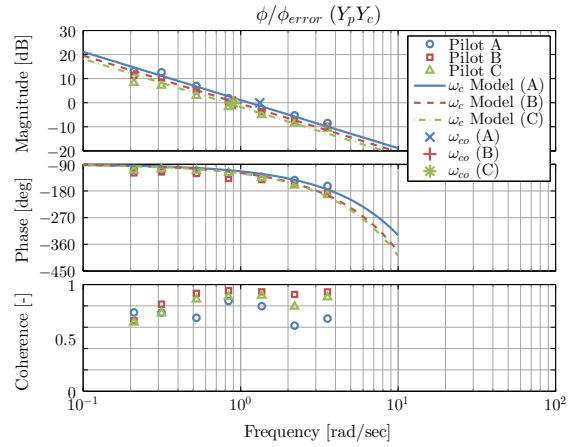


Figure 41. Roll tracking pilot-vehicle describing function variations (M0.3/5000 ft, Nominal loading configuration, Pilots A-C).

at lower frequencies for this task with higher stability margins. The average PVS crossover frequency for the roll tracking task was $\omega_c = 0.97$ rad/sec, as compared to $\omega_c = 2.13$ rad/sec for the pitch tracking task, indicating that with the larger error tolerance to meet desired performance in roll than in pitch, the roll tracking task bandwidth is around $\omega_T \approx 1.0$ rad/sec. For the roll tracking task, the pilot cutoff frequency ω_{co} tracks the PVS crossover frequency ω_c well.

Figure 43 shows the aircraft roll attitude response (Y_c) for the three pilots, evaluated at the discrete sum-of-sines frequencies, as well as the linear model roll attitude response. As with the pitch axis, the roll attitude bandwidth of the control laws is set by the command model. In the roll axis, the first-order command model time constant was set to match the bare-airframe's roll mode time constant, τ_r , which meets the Level 1 roll attitude bandwidth requirement $\omega_{BW} \geq 1.0$ rad/sec.²³ For this flight condition, the aircraft roll attitude bandwidth is $\omega_{BW} = 2.5$ rad/sec, as shown in Figure 43. As with the pitch tracking task, this value of aircraft roll attitude bandwidth allowed the pilots to operate at frequencies above the task bandwidth and achieve desired performance with minimal workload and Level 1 HQRs.

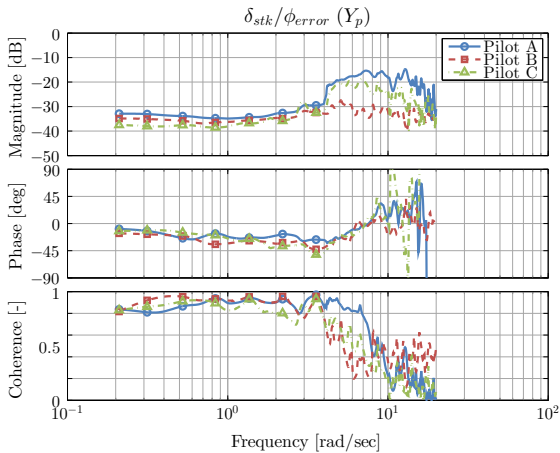


Figure 42. Roll tracking pilot describing function variations (M0.3/5000 ft, Nominal loading configuration, Pilots A-C).

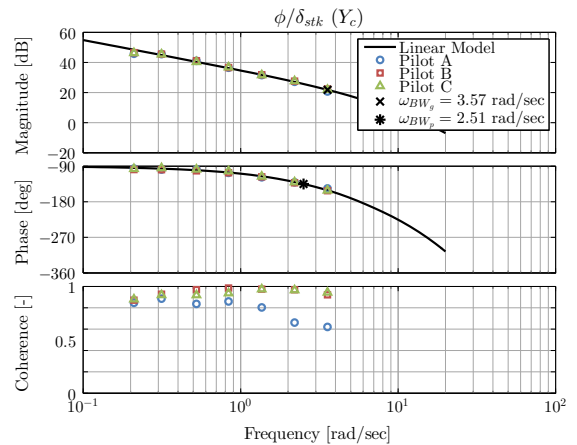


Figure 43. Roll tracking vehicle describing function variations (M0.3/5000 ft, Nominal loading configuration, Pilots A-C).

Table 6. Pilot-Vehicle Parameters for Roll Tracking Task

	Pilot A	Pilot B	Pilot C
<i>Pilot-Vehicle Parameters ($Y_p Y_c$)</i>			
Crossover Frequency ω_c [rad/sec]	1.14	0.95	0.81
Equivalent Time Delay τ [sec]	0.42	0.51	0.54
Gain Margin [dB]	10.40	10.17	11.11
Phase Margin [deg]	62.81	62.08	64.95
<i>Pilot Parameters (Y_p)</i>			
Cutoff Frequency ω_{co} [rad/sec]	1.32	0.92	0.90
Pilot Gain K_p	0.022	0.018	0.015
Time Delay τ_p [sec]	0.15	0.26	0.29

E. Precision Landing

Figure 44 shows the pilot HQRs for the precision landing task for the different loading configurations and turbulence levels tested. For the nominal loading configuration, pilots gave consistent ratings for the two levels of turbulence. Pilots noted that for the ambient turbulence cases, they could meet desired performance (as shown in Figure 45) with good precision and without having to be aggressive. With moderate turbulence, they could meet desired performance (as shown in Figure 45), but required “a little more attention and control input,” although this was deemed as normal control technique. The HQRs are the same for the two different levels of turbulence, because the critical sub-phase of the task was responding to the angle-of-attack gust which had the same magnitude regardless of turbulence level.

The off-nominal loading configuration received one Level 2 rating because the pilot noted that this configuration had no apparent speed stability (i.e. the nose did not pitch down when the airspeed dropped below the reference airspeed). This was because for this loading configuration, the $n_z u$ integrator in the longitudinal control laws, which provides the speed stability, was more likely to limit. This is addressed in more detail in Section VI.C.

Figure 46 shows an example of one of the data runs for the nominal weight/CG configuration with moderate turbulence. For this run, the pilot was able to maintain the glideslope and airspeed within the desired bounds on the approach phase. There was one minor excursion outside of the adequate bounds on the glideslope (section in red on the second plot in Figure 46), however this corresponds to when the angle-of-attack gust was applied, and the pilot was able to quickly get back onto the desired glideslope. For the touchdown phase of the run, the pilot was able to touch down within the desired box and with a desired sink rate. The remainder of the precision landing task runs had similar performance to the one shown in Figure 46.

Figure 47 shows the actuator rate RMS and peak values during the precision landing tasks, and Figure 48 shows actuator rate time histories for one of the precision landing runs at the light-weight/aft-CG loading configuration with moderate turbulence. As expected, the RMS values for all of the actuators increase going from ambient turbulence to moderate turbulence and from the nominal loading configuration to the light-weight/aft-CG loading configuration. However, all actuator rate RMS values are below 5 deg/sec. The highest actuator rate peak value observed was for the elevator actuator in the light-weight/aft-CG loading configuration, and was $\dot{\delta}_{elev} \approx 27$ deg/sec. As seen in Figure 48, the elevator actuator peak rate was one spike in response to the angle of attack gust at around $t = 60$ sec. The remaining peaks are closer to the aileron actuator values of $\dot{\delta}_{ail} \approx 15$ deg/sec. As with the tracking tasks, the actuator rates seen for the precision landing task are well within rate limits for standard hydraulic actuators with the loads seen at these flight conditions.

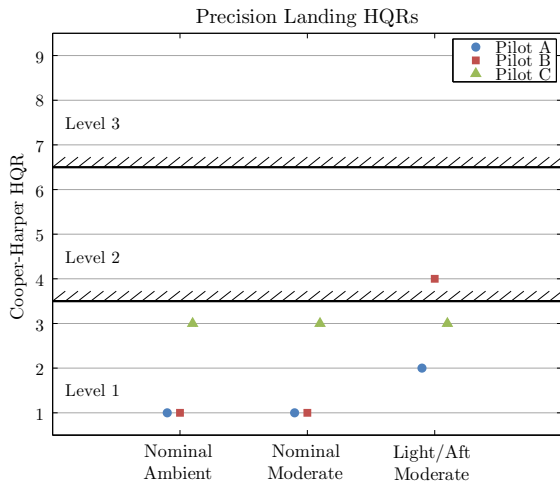


Figure 44. Precision landing HQRs.

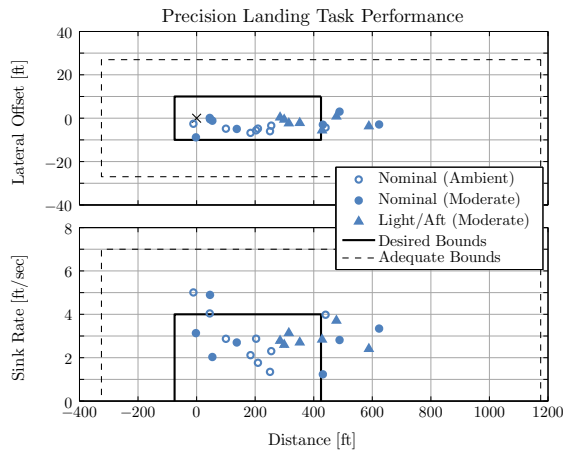


Figure 45. Precision landing task performance.

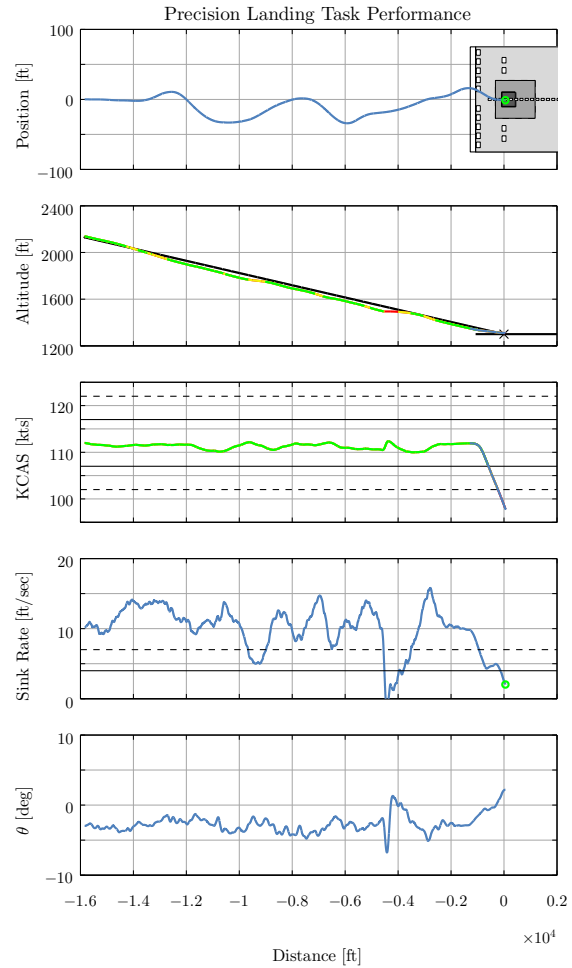


Figure 46. Example precision landing performance.

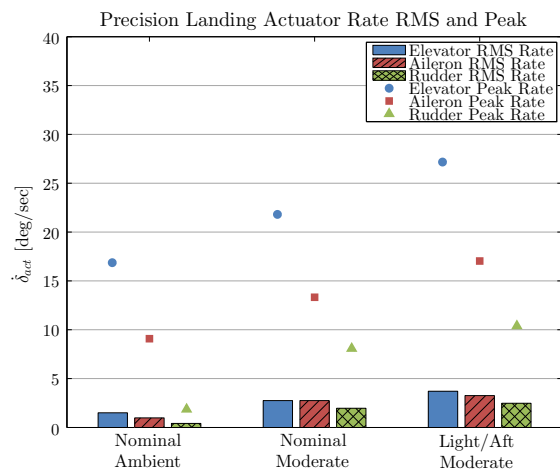


Figure 47. Actuator rate RMS and peak values during precision landing tasks.

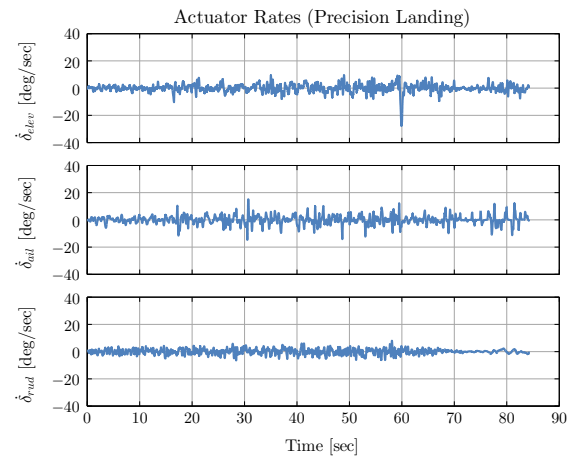


Figure 48. Example actuator rates during precision landing.

F. Lateral Offset Precision Landing

Figure 49 shows the pilot HQRs for the lateral offset precision landing task for the different loading configurations and turbulence levels tested. The ratings are all Level 1, demonstrating that the handling qualities of the control laws are robust to changes in loading configuration. Pilots commented that they could meet the desired performance for all of the conditions tested. Figure 50 shows the task performance for the different conditions tested, with nearly all cases falling within the desired bounds.

For the nominal loading configuration in ambient turbulence, pilots commented that they were able to be aggressive, had good level of precision, and that the predictability of the aircraft responses was “very good” and “very consistent.” For the nominal loading configuration in moderate turbulence, pilots noted that airplane responsiveness and predictability were the same, although the approach phase of the task required a higher workload. The offset correction was the same, due to similar magnitudes of lateral gusts being applied at the correction point for both levels of turbulence.

For the heavy-weight/aft-CG configuration in moderate turbulence, pilots commented that the handling, performance, and predictability were very similar to the nominal loading configuration. One pilot noted having to apply a little more back pressure on the stick during the flare for the heavy configuration. Furthermore, Pilot B noted that the lateral gust was less noticeable for this configuration, and hence the improvement of one HQR between the nominal loading configuration and heavy-weight/aft-CG configuration.

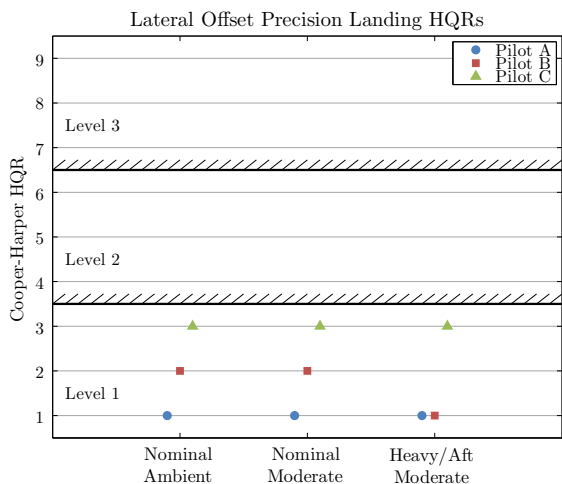


Figure 49. Lateral offset precision landing HQRs.

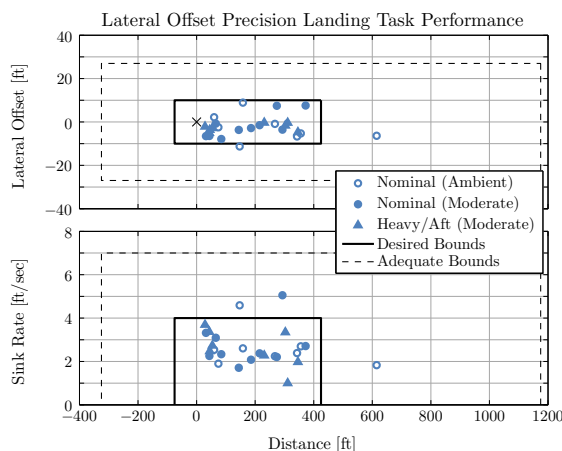


Figure 50. Lateral offset precision landing task performance.

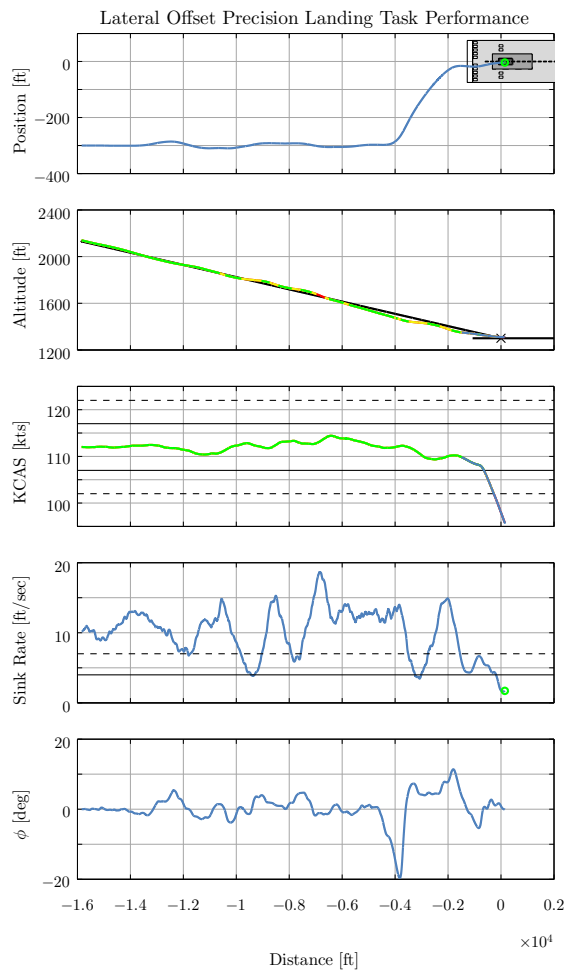


Figure 51. Example lateral offset precision landing performance.

Figure 51 shows an example of one of the data runs for the nominal weight/CG configuration with moderate turbulence. For this run, the pilot touched down within the desired box and with a desired sink

rate, and maintained the glideslope and airspeed within the desired bounds. The remainder of the offset landing runs had similar performance to that shown in Figure 51.

Figure 52 shows the actuator rate RMS and peak values during the lateral offset precision landing tasks, and Figure 53 shows actuator rate time histories for one of the lateral offset precision landing runs at the nominal loading configuration with moderate turbulence. As expected, the RMS values for all of the actuators increase going from ambient turbulence to moderate turbulence and decrease slightly going from the nominal loading configuration to the heavy-weight/aft-CG loading configuration. However, all actuator rate RMS values are below 5 deg/sec. The highest actuator rate peak value observed was for the aileron actuator in the nominal loading configuration under moderate turbulence, and was $\dot{\delta}_{ail} \approx 24$ deg/sec. As seen in Figure 53, the aileron and rudder actuator peak rates were in response to the lateral gust at around $t = 55$ sec. As with the tracking tasks, the actuator rates seen for the lateral offset precision landing task are well within rate limits for standard hydraulic actuators with the loads seen at these flight conditions.

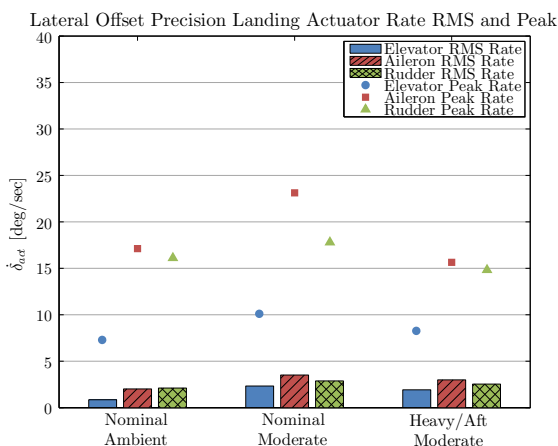


Figure 52. Actuator rate RMS and peak values during lateral offset precision landing tasks.

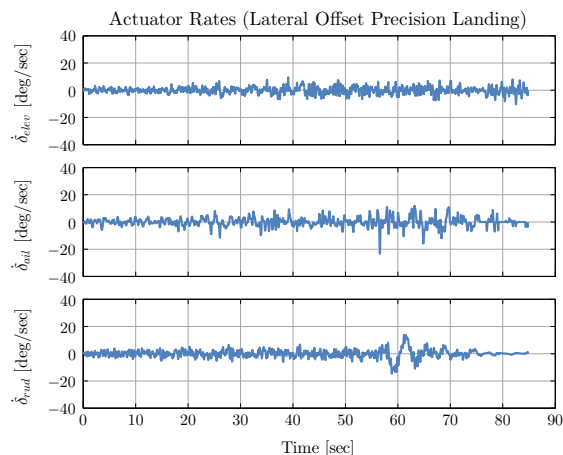


Figure 53. Example actuator rates during lateral offset precision landing.

G. Bare-Airframe Results

In order to compare the performance of the FBW control system to that of the bare-airframe, the lateral offset precision landing task was flown with both configurations. Figure 54 shows the pilot HQRs for the lateral offset precision landing task for the FBW control laws and the bare-airframe for two different levels of turbulence. As presented in Section V.F, the FBW control laws received Level 1 ratings for this task. In the case of the bare-airframe, two of the pilots gave Level 2 ratings, and one pilot gave Level 1 ratings.

Pilot A noted that although he could still meet desired performance with the bare-airframe, he did not have the same level of precision as with the FBW control system. Additionally, Pilot A noted that he could be more aggressive with the FBW control system than with the bare-airframe due to the tighter response given by the control system. During his evaluation of the bare-airframe, Pilot A noted that the friction force in the wheel was too high and the wheel would not center, requiring a bit of control hunting in the roll axis. This was more noticeable in the ambient turbulence case, and was masked by the higher turbulence of the moderate turbulence case. Hence Pilot A's improved HQR going from ambient to moderate turbulence for the bare-airframe evaluation.

Pilot B noted that he could not be very aggressive in the roll axis, and precision was not as good for maintaining wings level for the bare-airframe as compared to the FBW control laws.

Pilot C commented that with the bare-airframe, he was continuously working on the approach phase of the task, similar to the tracking tasks he had flown. Because of this, the workload for the task was higher with the bare-airframe than with the FBW control system and the critical sub-phase of the task while flying the bare-airframe became flying through turbulence for the whole task, as opposed to the offset correction for flying with the FBW control system. Furthermore, Pilot C noted that there was a medium level of precision with the bare-airframe, as opposed to high level of precision with the FBW control system.

Figure 55 shows the task performance for the lateral offset precision landing task for the FBW control

laws and the bare-airframe for two different levels of turbulence. The performance levels are similar for the two configurations, with the bare-airframe having more runs outside of desired performance, consistent with the pilot comments that it had a lower level of precision than the FBW control laws.

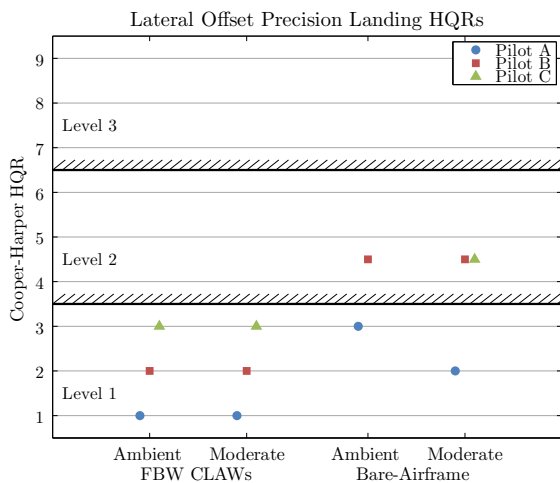


Figure 54. Lateral offset precision landing HQRs.

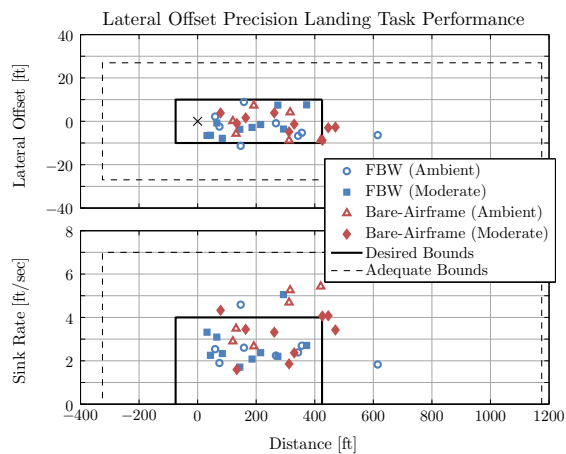


Figure 55. Lateral offset precision landing task performance.

VI. Discussion

A. Control Law Optimization

The FBW control laws received Level 1 HQRs for the roll tracking, precision landing, and lateral offset precision landing tasks, and borderline Level 1/Level 2 HQRs for the pitch tracking task, while modeling real world issues including actuator rate and position limits, integrator anti-windup, system delays, and atmospheric disturbances. Pilots commented that the FBW control laws were very predictable and that they used normal control techniques to complete the tasks, without the need for any pilot retraining or adaptation. Nor did the control laws exhibit any unusual responses, such as abnormal control movements, PIO tendencies, or limit cycle oscillations for the tasks tested. Actuator rates observed during the tasks were well within rate limit values of standard hydraulic actuators, and actuator rate limiting was not an issue, as predicted by the OLOP criteria used in the control law optimization. When compared to the bare-airframe, the FBW control laws provided increased ability to be aggressive, better precision, and improved task performance for the offset landing.

The performance and Level 1 ratings of the FBW control laws during the handling qualities demonstration maneuvers used in this study validates the specification-driven optimization-based approach to flight control design used to develop the control laws.^{1,2} The list of specifications used in the control law development is reproduced for reference in Appendix C. Furthermore, performance and HQRs did not vary with flight condition or aircraft loading configuration, thus validating the performance robustness of the control laws designed by using a multi-model optimization approach and by enforcing a minimum crossover frequency in each axis in the control laws.

B. Tracking Tasks

The control laws received borderline Level 1/Level 2 ratings for the pitch tracking task, which pilots deemed too aggressive for an aircraft of this class. In order to achieve desired performance for the pitch tracking task, pilots were operating at an average pilot-vehicle open-loop crossover frequency of $\omega_c = 2.13$ rad/sec, 70% greater than the pitch attitude bandwidth specification of $\omega_{BW} \geq 1.25$ rad/sec, but well below the installed closed-loop pitch attitude aircraft bandwidth of $\omega_{BW} = 4.33$ rad/sec.

In contrast, the roll tracking task which used wider performance bounds due to the available display, was deemed more suitable for a business jet by the pilots. In order to achieve desired performance for the roll tracking task, pilots were operating at an average pilot-vehicle open-loop crossover frequency of

$\omega_c = 0.96$ rad/sec, roughly equal to the roll attitude bandwidth specification of $\omega_{BW} \geq 1.0$ rad/sec, but well below the installed closed-loop roll attitude bandwidth of $\omega_{BW} = 2.5$ rad/sec. This supports the bandwidth specification value.

In both pitch and roll, the installed aircraft bandwidth, a function of the command model used in the control laws and the control laws' robust model following performance, is greater than the minimum attitude bandwidth requirements and the pilots' operating frequencies while performing the tracking tasks. This allowed the pilots to achieve desired performance for the tracking tasks with sufficient stability margins while acting in a pure-gain fashion.

C. Integrator Limiting in the Landing Task

Aside from the pitch tracking task, which pilots commented was too aggressive for an aircraft of this class, the FBW control system received only one Level 2 rating—an HQR 4 for the landing task in the light-weight/aft-CG configuration. The pilot who assigned this rating commented that the aircraft appeared to have no speed stability in this configuration, i.e., as he would slow below the reference airspeed, the aircraft would not pitch down to increase speed. This was only noted at the light/aft loading configuration, and was investigated further. As described in Section II.B.4, the control laws include a trim lookup table that is a function of flight condition and flap angle only. Ignoring the forward path contribution of the control laws, the commanded elevator deflection, $\delta_{elev_{cmd}}$, is given by:

$$\delta_{elev_{cmd}} = \delta_{elev_0} + K_{\dot{\alpha}}(\dot{\alpha}_{cmd} - \dot{\alpha}) + K_{\alpha}(\alpha_{cmd} + \alpha_0 - \alpha) + \frac{K_I}{s}(n_{z_{cmd}} + K u_{err} + \cos \gamma - n_z) \quad (6)$$

Where, δ_{elev_0} and α_0 are the trim elevator position and angle-of-attack for the nominal loading configuration from lookup tables in the control laws.

During trim flight condition at the nominal loading configuration, with no input on the stick, $\dot{\alpha}_{cmd} = \alpha_{cmd} = n_{z_{cmd}} = 0$, $\alpha = \alpha_0$, $n_z = \cos \gamma$, $u_{err} = 0$, $\delta_{elev_{cmd}} = \delta_{elev_0}$, and the integrator output is 0. At an off-nominal loading configuration, such as the light-weight/aft-CG configuration, in trim flight, $\dot{\alpha}_{cmd} = \alpha_{cmd} = n_{z_{cmd}} = 0$, $n_z = \cos \gamma$, and $u_{err} = 0$, however, $\alpha = \alpha_{trim} \neq \alpha_0$ and $\delta_{elev_{cmd}} = \delta_{elev_{trim}} \neq \delta_{elev_0}$. Therefore, the integrator must hold a steady-state value of:

$$\frac{1}{s_{ss}} = \frac{\delta_{elev_{trim}} - \delta_{elev_0} - K_{\alpha}(\alpha_0 - \alpha_{trim})}{K_I} \quad (7)$$

As described in Section II.B.7, the integrators in the control system are limited to prevent integrator windup, with the longitudinal axis integrator limited to command ± 10 deg of elevator deflection. However, if the steady-state contribution of the integrator, given in Equation 7, is large, then the integrator might limit for small airspeed errors, which was the case for the light-weight/aft-CG configuration in the approach condition.

There are several ways to mitigate this issue. One such method is a Differential PI-Algorithm (DPIA) used on the Eurofighter,²⁴ which differentiates all proportional feedback loops and all direct command path inputs to the surfaces, and then subsequently integrates them, thus removing steady-state trim error contributions. Alternatively, the integral path limit may be increased to the full elevator authority, or logic may be introduced to limit the integrator only when the elevator nears its limits. In this case, however, a simpler method was investigated in which a washout filter with a time constant of $\tau = 10$ sec was added to the angle-of-attack error signal:

$$\begin{aligned} \delta_{elev_{cmd}} &= \delta_{elev_0} + K_{\dot{\alpha}}(\dot{\alpha}_{cmd} - \dot{\alpha}) + \frac{s}{s + 0.1} K_{\alpha}(\alpha_{cmd} + \alpha_0 - \alpha) \\ &\quad + \frac{K_I}{s}(n_{z_{cmd}} + K u_{err} + \cos \gamma - n_z) \end{aligned} \quad (8)$$

Thus making the steady-state contribution of the integral path for off-nominal loading configurations a smaller value of:

$$\frac{1}{s_{ss}} = \frac{\delta_{elev_{trim}} - \delta_{elev_0}}{K_I} \quad (9)$$

Figures 56 and 57 show the effect of the angle-of-attack error signal washout filter on nominal and light-weight/aft-CG configurations, respectively. For the nominal configuration in trim (first 20 sec of the time history), the contribution of the proportional error path to the elevator command is $\delta_{e_P} = 0$ deg, and therefore the contribution of the integral path is, $\delta_{e_I} = 0$ deg both with and without the washout filter. For the light-weight/aft-CG configuration without the washout filter, in trim the contribution of the proportional error path to the elevator command is $\delta_{e_P} \approx 4$ deg and therefore $\delta_{e_I} \approx -8$ deg, close to the integral path limit of ± 10 deg. With the washout filter however, $\delta_{e_P} = 0$ deg and $\delta_{e_I} \approx -4$ deg.

Although the integral path limit is sufficient to hold trim for the off-nominal loading configurations, it is not enough to provide speed stability for a 10% reduction in throttle for the light-weight/aft-CG loading configuration, as shown in the last 120 sec of the time histories in Figures 56 and 57. For the nominal loading configuration (Figure 56), the aircraft response is nearly unchanged by the addition of the washout filter. For the light-weight/aft-CG configuration (Figure 57), without the washout filter, the integral path δ_{e_I} saturates after about 12 sec (at $t = 32$ sec), and the aircraft response diverges. At that point, the pilot must get in the loop to recover by either pitching the aircraft down or increasing the throttle. With the washout filter, however, the aircraft regains speed stability, and behaves like it does for the nominal loading configuration.

The addition of the washout filter was further analyzed using time simulations of the model in turbulence, and by including it in the linear model and evaluating the control system performance against the design specifications in CONDUIT[®]. The washout filter was found to have no negative impact on the control laws. Finally, at the end of the experiment, the pilots were asked to fly the precision landing task with and without the washout filter in the control laws. Pilots noted no difference between the two cases for the nominal configuration. For the light-weight/aft-CG configuration, the pilot who noticed the lack of speed stability in the case with no washout filter, noted that speed stability was restored and the aircraft behaved as expected with the washout filter.

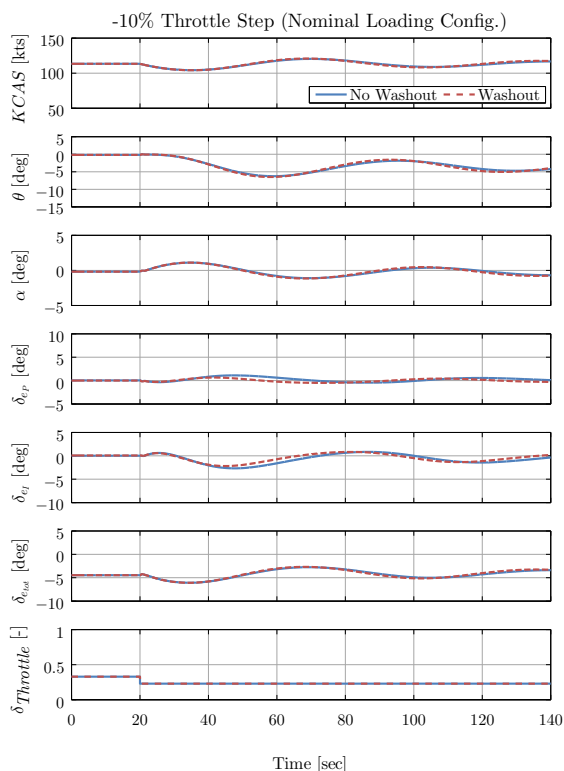


Figure 56. Throttle step response for nominal loading configuration.

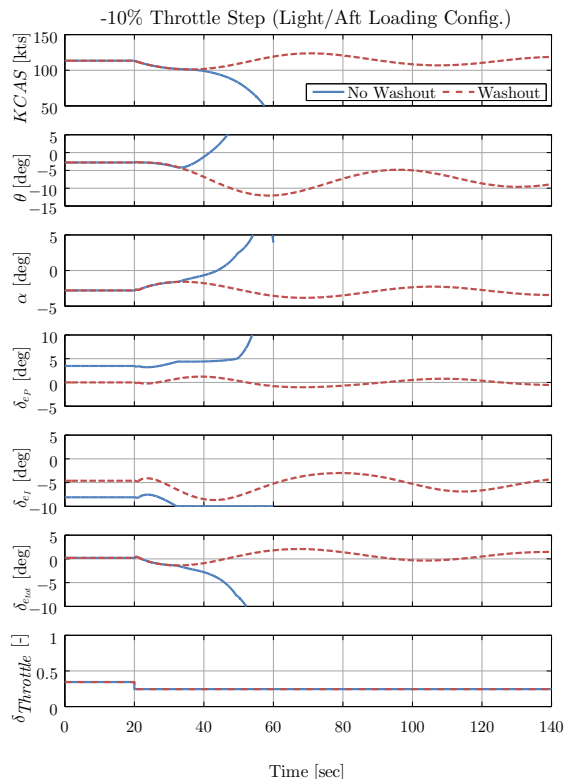


Figure 57. Throttle step response for light-weight/aft-CG loading configuration.

VII. Conclusions

1. The implementation of the simulation model using a continuous, full-envelope stitched model as well as control law gain lookup tables, was validated using frequency sweep techniques. The data were analyzed using frequency domain system identification methods and compared to the linear point models, with the closed-loop, broken-loop, and disturbance responses all matching very well.
2. The performance and overall Level 1 rating of the FBW control laws in a piloted simulation environment validates the specification-driven optimization approach to flight control designed used to develop the control laws. In addition, performance and HQRs did not vary with flight condition or aircraft loading configuration, thus validating the performance robustness of the control laws designed by using a multi-model optimization approach and by enforcing a minimum crossover frequency in each axis in the control laws.
3. While lateral/directional off-axis feed-forward gains where designed to provide proverse off-axis responses, they required tuning in the simulator for good handling qualities. In addition, sidestick command shaping and the aircraft flare characteristics (g-command per kt-error) were tuned in the simulator prior to the handling qualities experiment.
4. The sum-of-sines tracking tasks were used to analyze pilot crossover and cutoff frequencies and compare them to the task bandwidth and the control law attitude bandwidth. Pitch and roll attitude bandwidths were well in excess of the minimum handling qualities requirements for aircraft bandwidth, and thus allowed the pilots to complete the tracking tasks with Level 1 HQRs while operating in a pure-gain fashion. The good agreement of the cutoff and crossover frequencies trends validates the use of the former to quantify the pilot-vehicle system when the forcing function is not available.
5. Integrator limits were generally not reached during the maneuvers tested, except in the longitudinal axis for the approach flight condition and light-weight/aft-CG loading configuration. The issue was overcome by including a low-frequency washout filter on the proportional angle-of-attack error feedback signal. This restored speed stability to the light-weight/aft-CG loading configuration, while having no negative impact on the nominal loading configuration.

Acknowledgments

The authors would like to thank Corey Eckhart for his help with refinement of the test maneuvers used in this experiment, as well as Jim Hammer for his help with simulator integration. Furthermore, the authors would like to thank the test pilots who participated in this study, Peter Fisher, MAJ Joseph Minor, and Jason Rew, for providing their time, insight, and excellent comments.

References

- ¹Berger, T., Tischler, M. B., Hagerott, S. G., Gangsaas, D., and Saeed, N., "Longitudinal Control Law Design and Handling Qualities Optimization for a Business Jet Flight Control System," presented at the AIAA Atmospheric Flight Mechanics Conference, Minneapolis, MN, August 2012.
- ²Berger, T., Tischler, M. B., Hagerott, S. G., Gangsaas, D., and Saeed, N., "Lateral/Directional Control Law Design and Handling Qualities Optimization for a Business Jet Flight Control System," presented at the AIAA Atmospheric Flight Mechanics Conference, Boston, MA, August 2013.
- ³Tischler, M. B., Ivler, C. M., Mansur, M. H., Cheung, K. K., Berger, T., and Berrios, M., "Handling-Qualities Optimization and Trade-offs in Rotorcraft Flight Control Design," presented at the Rotorcraft Handling Qualities Conference, University of Liverpool, UK, November 2008.
- ⁴Anon., "Flight Control Design - Best Practices," NATO RTO-TR-029, December 2000.
- ⁵Pratt, R. W., "Flight Control Systems," AIAA Progress in Astronautics and Aeronautics, Vol. 184, 2000.
- ⁶Anon., "Flying Qualities of Piloted Aircraft," MIL-STD-1797B, Department of Defense Interface Standard, February 2006.
- ⁷Klyde, D. H. and Mitchell, D. G., "Handling Qualities Demonstration Maneuvers for Fixed-Wing Aircraft, Volume II: Maneuver Catalog," WL-TR-97-3100, October 1997.
- ⁸Tischler, M. B. and Remple, R. K., *Aircraft and Rotorcraft System Identification: Engineering Methods and Flight Test Examples Second Edition*, AIAA, 2012.
- ⁹Anemaat, W. A. J. and Kaushik, B., "Geometry Design Assistant for Airplane Preliminary Design," presented at the AIAA Aersopace Sciences Meeting, Orlando, FL, January 2011.

- ¹⁰Anon., "Type Certificate Data Sheet No. A1WI Rev. 19," Department of Transportation Federal Aviation Administration, 2011.
- ¹¹Tobias, E. L., Tischler, M. B., Berger, T., and Hagerott, S. G., "Full Flight-Envelope Simulation and Piloted Fidelity Assessment of a Business Jet Using a Model Stitching Architecture," presented at the AIAA Modeling and Simulation Technologies Conference, Kissimmee, FL, January 2015.
- ¹²Gangsaas, D., Hodgkinson, J., Harden, C., Saeed, N., and Chen, K., "Multidisciplinary Control Law Design and Flight Test Demonstration on a Business Jet," presented at the AIAA Guidance, Navigation, and Control Conference and Exhibit, Honolulu, HI, August 2008.
- ¹³Anon., "Airworthiness Standards: Transport Category Airplanes," Code of Federal Regulations, Title 14, Part 25, Department of Transportation Federal Aviation Administration, January 2004.
- ¹⁴Adams, R. J., Buffington, J. M., Sparks, A. G., and Banda, S. S., *Robust Multivariable Flight Control*, Springer-Verlag, 1994.
- ¹⁵Blight, J. D., Calderia, F. R., and Gangsaas, D., "Control Law Development for Aircraft An Example of Industry Practices," presented at the American Control Conference, Seattle, WA, June 2008.
- ¹⁶National Research Council, *Aviation Safety and Pilot Control: Understanding and Preventing Unfavorable Pilot-Vehicle Interactions*, National Academy Press, 1997.
- ¹⁷Anon., "Flight Test Guide For Certification of Transport Category Airplanes," Advisory Circular 25-7c, Department of Transportation Federal Aviation Administration, October 2012.
- ¹⁸Cooper, G. E. and Harper, R. P., "The Use of Pilot Rating in the Evaluation of Aircraft Handling Qualities," NASA TN D-5153, April 1969.
- ¹⁹Hovmark, G., Mehl, H. J., Smaili, H., and Crouzet, M., "Test Techniques For Experimental Detection of PIO," GARTEUR/TP-120-03, May 2000.
- ²⁰Atencio, A., "Fidelity Assesment of a UH-60A Simulation on the NASA Ames Vertical Motion Simulator," NASA TM 104016, September 1993.
- ²¹Heffley, R. K., Bourne, S. M., Curtis, H. C., Hindson, W. S., and Hess, R. A., "Study of Helicopter Roll Control Effectiveness Criteria," NASA CR 177404, April 1986.
- ²²Fujizawa, B. T., Lusardi, J. A., Tischler, M. B., Braddom, S. R., and Jeram, G. J., "Response Type Tradeoffs in Helicopter Handling Qualities for the GVE," presented at the American Helicopter Society 67th Annual Forum, Virginia Beach, VA, May 2011.
- ²³Mitchell, D. G., Hoh, R. H., L., A. B., and H., K. D., "Proposed Incorporation of Mission-Oriented Flying Qualities into MIL STD-1797A," Report No. WL-TR-94-3162. Wright-Patterson Air Force Base, Ohio: Wright Laboratory, October 1994.
- ²⁴Osterhuber, R., Hanel, M., and Hammon, R., "Realization of the Eurofighter 2000 Primary Lateral/Directional Flight Control Laws with Differential PI-Algorithm," presented at the AIAA Guidance, Navigation, and Control Conference, Providence, RI, August 2004.

Appendix A Pilot Questionnaire

Task Performance

1. Describe ability to meet DESIRED / ADEQUATE performance standards.
2. Rate your ability to be aggressive.
3. Rate the level of precision.
4. If trying for DESIRED performance resulted in unacceptable oscillations, did decreasing your goal to ADEQUATE performance alleviate the problem?
5. If unacceptable oscillations were present, use the PIO Rating Scale.

Aircraft Characteristics

6. Describe any objectionable controller force characteristics.
7. Describe predictability of initial aircraft response.
8. Describe any mid- to long-term response problems.
9. Describe any objectionable oscillations or tendency to overshoot.
10. Describe any non-linearity of response.
11. Describe any problems with harmony of pitch and roll, speed control, with height control, and turn coordination.
12. Rate the predictability of aircraft response to pilot inputs:

Predictable						Unpredictable		
1	2	3	4	5	6	7	8	9

Demands on the Pilot

13. Describe overall control strategy in performing the task (cues used, scan, etc.).
14. Describe any control compensation you had to make you to account for deficiencies in the aircraft.
15. Describe any modifications you had to make to what you would consider normal control technique in order to make the aircraft behave the way you wanted.

MISC.

16. Please comment on anything else that may have influenced you.

Assign HANDLING QUALITIES RATING for overall task

17. Using the Cooper-Harper rating scale, please highlight your decision-making process and adjectives that are best suited in the context of the task. If assigned HQR is Level 2, briefly summarize any deficiencies that make this configuration unsuitable for normal accomplishment of this task, i.e., justify why the procuring activity should reject this configuration as a means to accomplish this task.
18. What was the critical sub-phase of the task (e.g., entry, steady-state, exit) or major determining factor in the overall Handling Quality Rating (HQR).

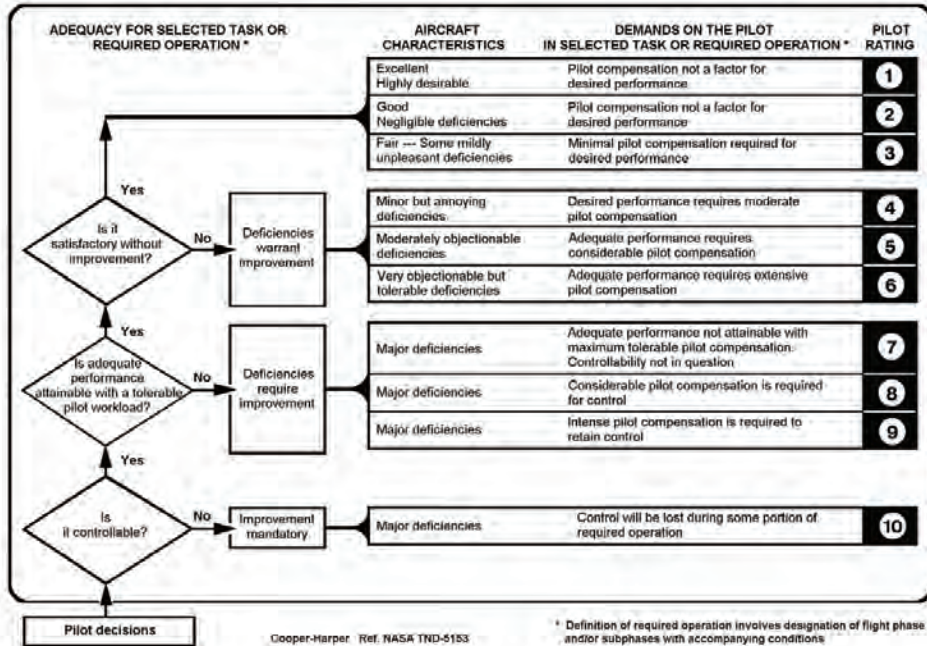


Figure 58. Cooper-Harper Handling Qualities Rating Scale.

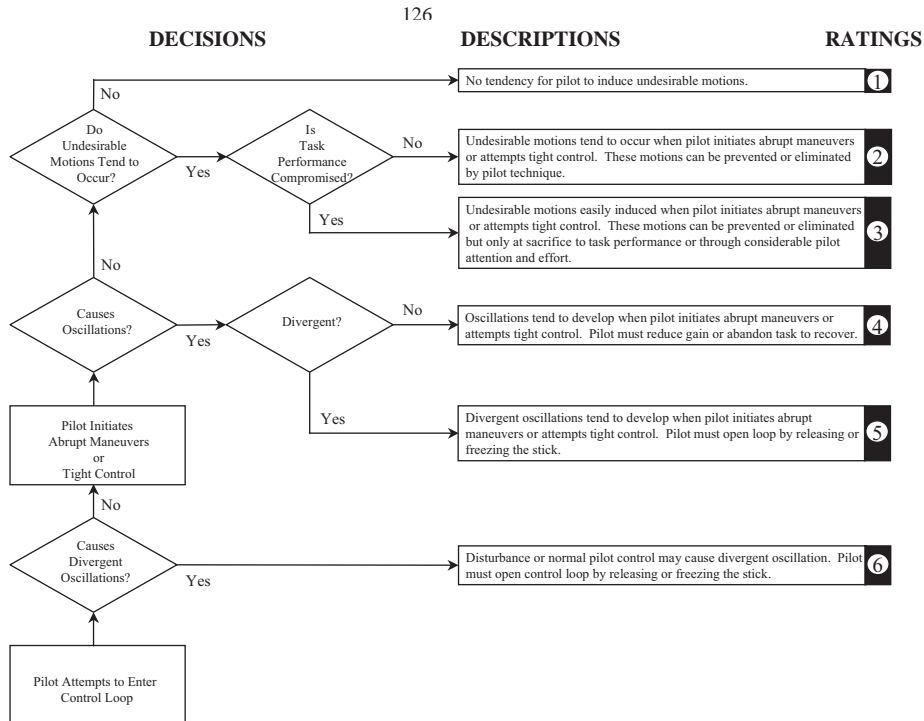


Figure 19. PIO tendency classification. Figure 59. PIO Tendency Classification Scale.

Ground-based simulation may or may not show up any PIO tendencies. Flight evaluation in variable-stability air vehicles is a valuable tool. Final determination will come from flight test of the actual vehicle.

Tom Twisdale provides some guidance on possible HQDT tasks:

35 of 38
 “Probably any test maneuver that allows the evaluation pilot to aggressively and assiduously track a precision time profile is a suitable HQDT test maneuver. In HQDT testing, the test maneuver is not nearly as important as the piloting technique. It is the piloting technique that increases the evaluation pilot's

Appendix B Test Matrix

Table 7. Complete Test Matrix

Task	Flight Condition	Loading Configuration	Turbulence	Control Laws
Pitch Capture	Mach 0.3/5000 ft	Nominal	None	FBW
Pitch Capture	Mach 0.3/5000 ft	Off-Nominal	None	FWB
Pitch Capture	Mach 0.58/FL350	Nominal	None	FWB
Pitch Capture	Mach 0.58/FL350	Off-Nominal	None	FWB
Roll Capture	Mach 0.3/5000 ft	Nominal	None	FWB
Roll Capture	Mach 0.3/5000 ft	Off-Nominal	None	FWB
Roll Capture	Mach 0.58/FL350	Nominal	None	FWB
Roll Capture	Mach 0.58/FL350	Off-Nominal	None	FWB
Pitch Tracking	Mach 0.3/5000 ft	Nominal	Ambient	FWB
Pitch Tracking	Mach 0.3/5000 ft	Off-Nominal	Ambient	FWB
Pitch Tracking	Mach 0.58/FL350	Nominal	Ambient	FWB
Pitch Tracking	Mach 0.58/FL350	Off-Nominal	Ambient	FWB
Roll Tracking	Mach 0.3/5000 ft	Nominal	Ambient	FWB
Roll Tracking	Mach 0.3/5000 ft	Off-Nominal	Ambient	FWB
Roll Tracking	Mach 0.58/FL350	Nominal	Ambient	FWB
Roll Tracking	Mach 0.58/FL350	Off-Nominal	Ambient	FWB
Precision Landing	Approach	Nominal	Ambient	FWB
Precision Landing	Approach	Off-Nominal	Ambient	FWB
Precision Landing	Approach	Nominal	Moderate	FWB
Precision Landing	Approach	Off-Nominal	Moderate	FWB
Lateral Offset Landing	Approach	Nominal	Ambient	FWB
Lateral Offset Landing	Approach	Off-Nominal	Ambient	FWB
Lateral Offset Landing	Approach	Nominal	Moderate	FWB
Lateral Offset Landing	Approach	Off-Nominal	Moderate	FWB
Lateral Offset Landing	Approach	Nominal	Ambient	Bare-Airframe
Lateral Offset Landing	Approach	Nominal	Moderate	Bare-Airframe

Appendix C Test Matrix

Table 8. Longitudinal Optimization Specifications

Constraint	Spec Name	Description (Motivation)	Domain*	Source	Config.†
<i>Tier 1</i>					
Hard	EigLcG1	Eigenevalues in L.H.P. (Stability)	S	Generic	N
	StbMgG1	Gain Phase Margin broken at elevator (Stability)	F	MIL-DLT-9490E	L,N,H
	NicMgG1	Nichols Margins broken at elevator (Stability)	F	GARTEUR	L,N,H
Soft	CapPiL2	CAP (short-period) (HQ)	L	MIL-STD-1797B	N
	FrqSpL5	ω_{sp} vs n/α (HQ)	L	MIL-STD-1797B	N
	TdlPiL1	Equivalent Time delay (HQ)	L	MIL-STD-1797B	N
	FrqSpC1	$\omega_{sp} \pm 25\%$ open-loop (Act. Activity)	L	Generic	N
	FrqTtC1	$T_{\theta_2} \pm 50\%$ open-loop (HQ, Act. Activity)	L	Generic	N
	CosLoG1	Max LOES Cost ($J \leq 10$) (HQ)	L	Generic	N
	FspGsL1	Stick force per g $\pm 2.5\%$ stick gain (HQ)	F	Generic	N
	FspKtL1	Stick force per kt $\pm 2.5\%$ stick gain (HQ)	F	Generic	N
	ModFoG2	Command model following cost (HQ)	F	Generic	L,N,H
	EigDpG1	Eigenvalue Damping (HQ, Loads)	S	Generic	N
	OlpOpG1	Open Loop Onset Point (PIO)	F	DLR	N
	DrpPiL1	Pitch dropback (HQ)	T	MIL-STD-1797B	L,N,H
	GstRpG1	Angle-of-attack gust response (Loads)	T	Generic	N
	DstBwG1	Dist. Rej. Bandwidth (Loads, Ride Quality)	F	ADS-33E	N
	DstPkG1	Dist. Rej. Peak (Loads, Ride Quality)	F	ADS-33E	N
	CrsMnG1	Minimum $\omega_c \geq 2.5$ rad/sec (Robustness)	F	Generic	N
	Summed	CrsLnG1	Crossover Frequency (Act. Activity)	F	Generic
Obj.	RmsAcG1	Actuator RMS (Act. Activity)	F	Generic	N
<i>Tier 2</i>					
Check Only	BnwPiL4	Bandwidth, phase delay (HQ)	F	MIL-STD-1797B	-
	BnwFpL1	Transient flight-path response (HQ)	F	MIL-STD-1797B	-
	NsmPiL1	Neal Smith (PIO)	F	AFFDL-TR-70-74	-
	GibPiL1	Gibson phase rate (PIO)	F	AGARD-CP-508	-
	NicMgG1	Nichols Margins broken at sensors (Stability)	F	GARTEUR	-

*F = Frequency domain specification, T = Time domain specification, L = LOES specification, S = s-plane

†N = Nominal weight/CG configuration only, L,N,H = Light, Nominal, and Heavy weight/CG configurations

Table 9. Lateral/Directional Optimization Specifications

Constraint	Spec Name	Description (Motivation)	Domain*	Source	Config.†
<i>Tier 1</i>					
Hard	EigLcG1	Eignevalues in L.H.P. (Stability)	S	Generic	N
	StbMgG1	Gain and phase margins loop broken at actuators and sensors (Stability)	F	MIL-DLT-9490E	L,N,H
	NicMgG1	Nichols Margins loop broken at actuators and sensors (Stability)	F	GARTEUR	L,N,H
Soft	FrqRoD4	Roll model time constant (HQ)	L	MIL-STD-1797B	N
	FrqDrD3	Dutch roll frequency (ω_{dr}) (HQ)	L	MIL-STD-1797B	N
	DmpDrD2	Dutch roll damping (ζ_{dr}) (HQ)	L	MIL-STD-1797B	N
	ReaDrD2	$\zeta_{dr}\omega_{dr}$ (HQ)	L	MIL-STD-1797B	N
	FrqRoC1	$\tau_r \pm 30\%$ open-loop (HQ, Act. Activity)	L	Generic	N
	FrqDrC1	$\omega_{dr} \pm 20\%$ open-loop (HQ, Act. Activity)	L	Generic	N
	CosLoG1	Max LOES Cost (HQ)	L	Generic	N
	EigDpG1	Eigenvalue Damping (HQ, Loads)	S	Generic	N
	OlpOpG1	Open Loop Onset Point (PIO)	F	DLR	N
	ModFoG2	Command model following cost (HQ)	F	Generic	L,N,H
	GstRpG1	Sideslip gust response (Loads)	T	Generic	N
	DstBwG1	Dist. Rej. Bandwidth (Loads, Ride Quality)	F	ADS-33E	N
	DstPkG1	Dist. Rej. Peak (Loads, Ride Quality)	F	ADS-33E	N
	MaxMgT1	Maximum tail loads during rudder kick, gust, and turbulence (Loads)	T	Generic	N
	CrsMnG1	Minimum $\omega_c \geq 3.5$ rad/sec (Robustness)	F	Generic	N
	Summed	CrsLnG1	Crossover Frequency (Act. Activity)	F	Generic
Obj.	RmsAcG1	Actuator RMS (Act. Activity)	F	Generic	N
<i>Tier 2</i>					
Check Only	TdlRoD1	Roll axis equivalent time delay (HQ)	L	MIL-STD-1797B	-
	TdlYaD1	Yaw axis equivalent time delay (HQ)	L	MIL-STD-1797B	-
	OscRoD4	Roll oscillations (HQ)	T	MIL-STD-1797B	-
	CouRsD2	Sideslip excursion (HQ)	T	MIL-STD-1797B	-
	PioRoD1	Roll PIO criteria (HQ)	T	MIL-STD-1797B	-
	TrnCrC1	Turn coordination (HQ)	T	Cessna	-
	OscRoD7	Roll rate transfer function zero cancellation	S	Generic	-
	InnRoD1	Innocenti lateral tracking	F	Innocenti	-

*F = Frequency domain specification, T = Time domain specification, L = LOES specification, S = s-plane

†N = Nominal weight/CG configuration only, L,N,H = Light, Nominal, and Heavy weight/CG configurations